

## Impacts of Meteorological Conditions, Aerosol Radiative Feedbacks, and Emission Reduction Scenarios on the Coastal Haze Episodes in Southeastern China in December 2013<sup>©</sup>

JIANQIONG ZHAN AND WENYUAN CHANG

*State Key Laboratory of Atmospheric Boundary Layer Physics and Atmospheric Chemistry, Institute of Atmospheric Physics, Chinese Academy of Sciences, Beijing, China*

WEI LI

*Key Laboratory of Global Change and Marine–Atmospheric Chemistry, Third Institute of Oceanography, State Oceanic Administration, Xiamen, China*

YANMING WANG

*Laboratory of Straits Meteorology, and Xiamen Meteorological Bureau, Xiamen, China*

LIQI CHEN AND JINPEI YAN

*Key Laboratory of Global Change and Marine–Atmospheric Chemistry, Third Institute of Oceanography, State Oceanic Administration, Xiamen, China*

(Manuscript received 22 June 2016, in final form 13 January 2017)

### ABSTRACT

Fujian Province in southeastern coastal China is a relatively clean region with low emissions, as its high altitude isolates it from the rest of the country. However, the region experienced haze episodes on 3–14 December 2013. The authors performed simulations using the Weather Research and Forecasting Model coupled with chemistry (WRF-Chem) to examine the impacts of meteorological conditions, aerosol radiative feedbacks (ARFs; including aerosol direct and nearly first indirect effect), and internal and external emissions reduction scenarios on particulate matter smaller than  $2.5\text{ }\mu\text{m}$  ( $\text{PM}_{2.5}$ ) concentrations. To the best of the authors' knowledge, this is the first time the WRF-Chem model has been used to study air quality in this region. The model reasonably reproduced the meteorological conditions and  $\text{PM}_{2.5}$  concentrations. The analysis demonstrated that the highest- $\text{PM}_{2.5}$  event was associated with a cold surge that promoted the impingement of northern pollutants on the region, and  $\text{PM}_{2.5}$  concentrations were sensitive to the emissions from the Yangtze River delta (16.6%) and the North China Plain (12.1%). This suggests that efforts toward coastal air quality improvement require regional cooperation to reduce emissions. Noticeably, ARFs were unlikely to increase  $\text{PM}_{2.5}$  concentrations in the coastal region, which was in contrast to the case in northern China. ARFs induced strong clean wind anomalies in the coastal region and also lowered the inland planetary boundary layer, which enhanced the blocking of northern pollutants crossing the high terrain in the north of Fujian Province. This indicates that ARFs tend to weaken the haze intensity in the southeastern coastal region.

---

### 1. Introduction

<sup>©</sup> Supplemental information related to this paper is available at the Journals Online website: <http://dx.doi.org/10.1175/JAMC-D-16-0229.s1>.

---

Corresponding author e-mail: Wenyuan Chang, changwy@mail.iap.ac.cn

Increasing anthropogenic emissions and weak East Asian winter monsoons have led to increased airborne particulate matter (PM) in eastern China, which has resulted in more frequent haze events in urban areas that diminish visibility and endanger human health (Niu

et al. 2010; Qu et al. 2010; Yang et al. 2011; X. Y. Zhang et al. 2012; Cheng et al. 2013). Air pollution episodes are commonly reported in high-emission areas in the North China Plain (NCP), the Yangtze River delta (YRD) region, and the Pearl River delta (PRD) region (Sun et al. 2014; Tang et al. 2016). In contrast, the ambient air is relatively clean in Fujian (FJ) Province, which is located between the rapidly developing YRD and PRD regions. Two major cities in Fujian Province, Xiamen ( $24.43^{\circ}\text{N}$ ,  $118.07^{\circ}\text{E}$ ), and Fuzhou ( $26.08^{\circ}\text{N}$ ,  $119.31^{\circ}\text{E}$ ), are ranked among the top 10 cleanest cities in China. However, during the eastern China extreme haze events of December 2013, when  $\text{PM}_{2.5}$  (PM smaller than  $2.5\ \mu\text{m}$  in diameter) concentrations exceeded  $200\ \mu\text{g m}^{-3}$  in the NCP and YRD regions (Yu et al. 2014; Jiang et al. 2015), extremely high PM levels were also observed in Fujian Province, with  $\text{PM}_{2.5}$  concentrations up to  $213\ \mu\text{g m}^{-3}$  in Xiamen (Yan et al. 2015).

Meteorological patterns play a vital role in the transport and mixing of particulate matter (Fast et al. 2012, 2014). Previous studies have observed aerosol chemical composition in southeastern coastal China and then demonstrated the potential for neighboring pollutants to impinge on coastal zones by backward trajectory analysis (Zhao et al. 2011; F. Zhang et al. 2012; Niu et al. 2013; Xu et al. 2013; Yin et al. 2014; Yan et al. 2015). Chuang et al. (2008) and Hsu et al. (2010) demonstrated that the winter extreme haze events in Taiwan and Kinmen Island in southeastern China have been induced by cold surges. The cold surges are characterized by high pressure, high wind speed, low temperature, and low relative humidity (Qu et al. 2015; S.-H. Wang et al. 2016). As cold surges propagate to the south, massive amounts of northern particulates are brought to the southeastern continental edge within a shallow layer approximately 1 km above the surface (Hsu et al. 2010; Yan et al. 2015; S.-H. Wang et al. 2016) and have consequently degraded air quality in the southeastern coastal region. This is different from the haze events in the NCP, where high  $\text{PM}_{2.5}$  concentrations have been suggested to be mainly due to accumulation of pollutants under stable weather conditions in winter (Zhao et al. 2013; Zhang et al. 2016a; Gao et al. 2015).

In general, large-scale transport of pollutants from the north to the south persists for several hours. It takes 28 h on average to transport particulates from the YRD region to northern Taiwan, which is 200 km east of Xiamen, according to the analysis of 36 winter haze events from 2005 to 2014 (S.-H. Wang et al. 2016). However, the extreme haze events in December 2013 persisted for around 10 days in Fujian (Yan et al. 2015), which means that these long-lasting air pollution events cannot be fully explained by large-scale transport. Hsu et al. (2010)

analyzed haze events on 6–9 December 2007 and 5–8 January 2008 at Kinmen Island, 8 km from Xiamen, and suggested that in addition to the transport of pollutants, the locally weak winds and lower mixing height could help maintain the high  $\text{PM}_{2.5}$  concentrations. This indicates that the buildup of high- $\text{PM}_{2.5}$  events in the south is related to several weather regimes.

In addition, aerosol radiative feedbacks are expected to exert an impact on meteorological parameters and, hence,  $\text{PM}_{2.5}$  concentrations. A few previous studies have indicated that aerosol radiative effects enhance the haze intensity by lowering the planetary boundary layer (PBL) height, as scattering aerosols cool the surface and black carbon heats the lower atmosphere, inducing a temperature inversion layer that traps more particles near the ground (Gao et al. 2014, 2015; Zhang et al. 2015; Ding et al. 2016). To date, studies on aerosol radiative effects have focused on stagnation days in high-emission areas (e.g., northern China), but whether that is the case for the relatively clean southeast coastal regions is not yet known.

Despite the efforts that have made to improve our understanding of the buildup of high-pollution events in China, most research has been focused in the NCP, PRD, or YRD regions. Previous studies in Fujian Province are usually based on observations. To understand the formation and buildup of the high- $\text{PM}_{2.5}$  episodes that occurred in Fujian Province, this study utilized the Weather Research and Forecasting Model coupled with chemistry (WRF-Chem) to investigate the impact of meteorological conditions, aerosol radiative feedbacks, and emission reduction scenarios on  $\text{PM}_{2.5}$  concentrations. To the best of our knowledge, air quality studies using WRF-Chem model simulations have not been applied in previous studies of this region.

The remainder of the paper is structured as follows: Section 2 describes the model configuration, experimental design, and observational data. The evaluation of the model performance is presented in section 3. We then investigate the linkage between meteorological conditions and time series variation of  $\text{PM}_{2.5}$  concentrations in section 4, we present how the aerosol radiative feedbacks impact  $\text{PM}_{2.5}$  concentrations under different meteorological conditions in section 5, and we conduct a sensitivity test to investigate how emission reductions by two major external contributing sources (NCP and YRD regions) and an internal source (Fujian) could affect  $\text{PM}_{2.5}$  concentrations in section 6. Section 7 summarizes our primary findings and the limitations of this work. The study highlights the linkage between the cold surge and the maximum high- $\text{PM}_{2.5}$  event in Fujian and shows that aerosol radiative feedbacks are unlikely to increase  $\text{PM}_{2.5}$  concentrations in the southeastern

coastal region, in contrast to significantly enhancing haze events in inland cities.

## 2. Methodology

### a. Model

The WRF-Chem model, version 3.6 (Grell et al. 2005; Fast et al. 2006; Gustafson et al. 2007), was used to investigate the factors, that is, meteorological conditions, aerosol radiative feedbacks, and emission reduction scenarios, affecting PM<sub>2.5</sub> concentrations. The simulations were configured in three two-way coupled nested domains with horizontal resolutions of 81, 27, and 9 km (Fig. 1a) and 27 vertical levels that extended from the surface to 50 hPa. The static geographical fields of terrain, soil properties, land use, and land cover were interpolated from 10-min (~19 km) U.S. Geological Survey data. Fujian Province is a mountainous province on China's southeastern coast (Fig. 1b), where concentrations of anthropogenic SO<sub>2</sub> (Fig. 1c) and other emission species (Fig. S1 in the online supplementary material; herein all supplemental figure, table, and equation numbers are preceded by an "S") are relatively low in comparison with those in the NCP and YRD regions. The relatively high altitude and rugged terrain isolate Fujian Province from the rest of the country (Fig. 1b), which makes it a relatively clean region with low levels of PM<sub>2.5</sub> [see Fig. 4 in Zhang et al. (2015)].

The physical options (listed in Table 1) used for this study included the Purdue Lin microphysics scheme of Lin et al. (1983), which explicitly resolves water vapor, cloud, and precipitation processes; the unified Noah land surface model (Chen and Dudhia 2001) to calculate the lower boundary conditions for vertical transport in the PBL; the asymmetric convective model, version 2 (ACM2), scheme (Pleim 2007) for PBL meteorological conditions; and the Rapid Radiative Transfer Model for General Circulation Models (RRTMG; Mlawer et al. 1997; Iacono et al. 2008) for short- and longwave radiation.

Gas-phase chemistry was simulated using the Carbon Bond Mechanism, version Z (CBMZ; Zaveri and Peters 1999; Fast et al. 2006), which includes aqueous-phase chemistry. The aerosol chemistry was based on the Model for Simulating Aerosol Interactions and Chemistry (MOSAIC; Zaveri et al. 2008) with four size bins. It is reasonable to believe that the four size bins might work well for options for transport and aerosol feedbacks associated with the direct effects, but they likely induce errors for aerosol microphysical effects on clouds because particle size affects cloud condensation nuclei and, hence, indirect effects (Abdul-Razzak and Ghan 2000, 2002). During the study period, the cloud cover is less than 2%,

and the mass ratios of cloudborne aerosols to total dry aerosols are as low as less than 1% in Xiamen, indicating an ignorable cloud–aerosol interaction in our simulations (Fig. S2 in the online supplementary material). Thus, the model biases induced by the four size bins are not expected to affect our analysis of aerosol radiative feedbacks. The simulated aerosols included sulfate, methanesulfonate, nitrate, ammonium, black carbon, primary organic carbon, sodium, calcium, chloride, carbonate, aerosol liquid water, and other inorganic matter (e.g., trace metals and silica). Secondary organic aerosols (SOAs), however, were not included in our MOSAIC aerosol module. Simulations including SOAs have been suggested to include a large uncertainty during haze events in China (R.-J. Huang et al. 2014; Jiang et al. 2012). Zhang et al. (2015) suggested that modeled SOAs only make up 2.8% of organic aerosols, and including SOAs does not increase the model performance of PM<sub>2.5</sub> during winter haze events in China. Excluding SOAs in the current model simulations would probably not substantially change the conclusions of the study. Aerosol optical properties were calculated as a function of wavelength based on the Mie theory. The aerosol components were internally mixed within a sectional bin and were externally mixed among the sectional bins. The mixed refractive indices were calculated using a volume-averaging approximation.

The initial and lateral boundary conditions for the meteorological fields were generated from the National Centers for Environmental Prediction (NCEP) Final Analysis (FNL) data using the GFS model at a horizontal resolution of 1° × 1°, while the initial and lateral boundary conditions for the chemical species were derived from time-specific chemical fields in the Model for Ozone And Related Chemical Tracers (MOZART; Emmons et al. 2010). The boundary conditions were updated every 6 h and then interpolated linearly in time by WRF-Chem. The sea surface temperature was updated every 6 h using the reanalysis data compiled by the U.S. Navy Fleet Numerical Meteorology and Oceanography Center. The four-dimensional data assimilation (nudging) technique was applied to domain 1 (Fig. 1a) to nudge the GFS reanalysis data throughout all the vertical levels, whereas domains 2 and 3 were free from the grid nudging and had two-way interaction with their parent domains in meteorological conditions at the lateral nudging zones. The advantage of this setup is to limit the large-scale meteorological errors during a long-term integration and allow full development of aerosol radiative feedbacks in domains 2 and 3.

Anthropogenic emissions from the 2010 MIX emission inventories were used ([www.meicmodel.org](http://www.meicmodel.org)), which included the multiresolution emission inventory

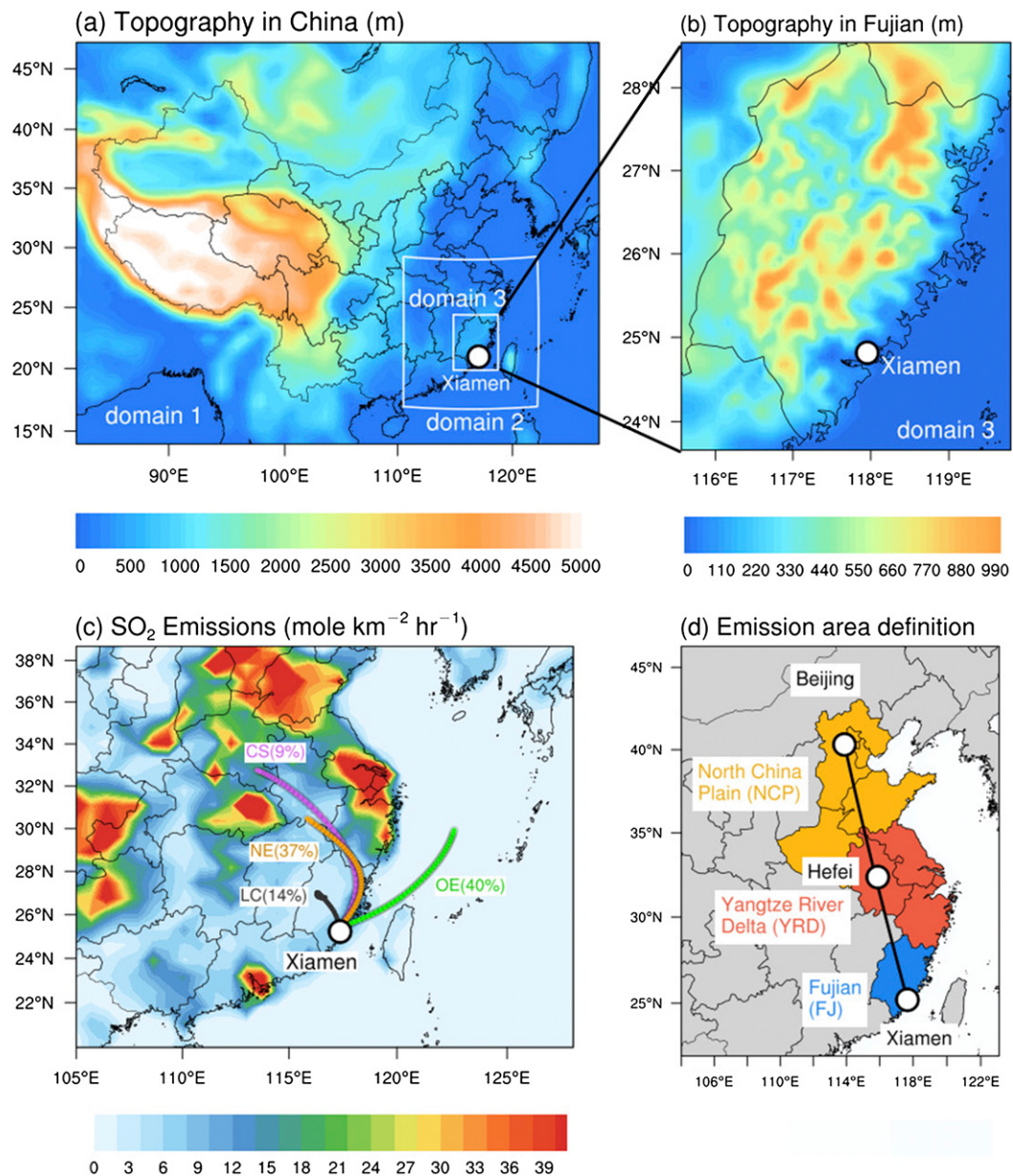


FIG. 1. (a),(b) The topography (m) of the study region and the model domains. (c) Anthropogenic  $\text{SO}_2$  emissions for 2010. The wintertime airmass transport pathways that affect the air quality of Xiamen on 1–14 Dec 2013 are shown (calculated by the HYSPLIT\_4 model). Four potential transport routes are identified in (c), with air masses related to clusters CS (9%), NE (37%), and LC (14%) and the ocean cluster OE (40%). The percentages denote the occurrence frequency of the pathways. (d) The emission areas discussed in the text. The anthropogenic emissions are eliminated in the NCP, YRD, and FJ to evaluate the impacts of neighboring emissions on Xiamen  $\text{PM}_{2.5}$  levels that are discussed in section 6. The black line denotes the cross section where the vertical  $\text{PM}_{2.5}$  concentrations are shown in Fig. 11, below.

of China (MEIC) and four other national or regional emission inventories covering East and South Asia (Li et al. 2017). It is reasonable to assume that trends in emissions likely affect concentrations to some extent, but there were no comprehensive open-access emission inventories for 2013 when this study was done. The

changes in emissions from 2010 to 2013 have not been considered in our study. The biogenic emissions were estimated using the Model of Emissions of Gases and Aerosols from Nature (MEGAN; Guenther et al. 2006). The biomass burning emissions were the Fire Inventory from NCAR, version 1 (FINN v1; Wiedinmyer et al.

TABLE 1. The WRF-Chem model configurations used in this study.

Physical and chemical process	Options
Four-dimensional data assimilation	Only operated in domain 1
Surface physics	Unified Noah land surface model
Boundary layer	ACM2
Longwave radiation	RRTMG
Shortwave radiation	RRTMG
Cumulus convection	Grell 3D scheme
Cloud microphysics	Lin et al. (1983)
Gas-phase chemistry	CBMZ
Photolysis	Madronich Fast-Tropospheric Ultraviolet and Visible model (F-TUV) photolysis
Aerosol chemistry	MOSAIC

2011), which presents the trace gas and particulate emissions from open biomass burning, including wildfire, agricultural fire, and prescribed burning, that were distributed vertically using an online plume rise module (Freitas et al. 2007) in the model. Anthropogenic, biogenic, and biomass burning emissions of  $\text{SO}_2$ ,  $\text{NO}$ ,  $\text{NH}_3$ , black carbon (BC), organic carbon (OC), and  $\text{CO}_2$  over China are shown in Fig. S1 and summarized in Table 2. Anthropogenic emissions in Fujian Province are relatively low when compared with those in the NCP. For example, anthropogenic  $\text{SO}_2$  in Fujian is  $1.58 \text{ Tg}(\text{SO}_2) \text{ yr}^{-1}$ , which is less than 10% of  $\text{SO}_2 [16.88 \text{ Tg}(\text{SO}_2) \text{ yr}^{-1}]$  emitted in the NCP. Biomass burning is strong in Fujian. The local biomass burning OC is up to  $0.20 \text{ Tg}(\text{OC}) \text{ yr}^{-1}$ , as compared with  $0.22 \text{ Tg}(\text{OC}) \text{ yr}^{-1}$  from anthropogenic sources. As high forest cover, biogenic emission is  $0.14 \text{ Tg}(\text{CO}) \text{ yr}^{-1}$  in Fujian, higher than the biogenic emissions in the NCP.

To investigate the impact of the meteorological conditions and emission reduction scenarios on  $\text{PM}_{2.5}$  concentrations, five simulations were conducted from 15 November to 30 December 2013 (Table 3). The first 6 days of each experiment were discarded as spinup. First, we performed a baseline experiment (DEF\_ANT\_RAD) with the default anthropogenic emissions of the 2010 MIX emission inventories and a full coupling between aerosols and meteorological variables. The second simulation was with aerosol radiative feedbacks (direct and first indirect) turned off (DEF\_ANT\_NORAD) in all the domains. The differences in meteorological conditions and  $\text{PM}_{2.5}$  concentrations between DEF\_ANT\_RAD and DEF\_ANT\_NORAD reflected the aerosol direct radiative effect and first indirect effect in DEF\_ANT\_RAD. Technically, a way to study the aerosol indirect effect is to fix cloud droplet condensation as described in Gustafson et al. (2007). During our

TABLE 2. Anthropogenic biomass burning and biogenic emissions in the NCP and FJ Province in December 2010.

Emissions	NCP ( $110^{\circ}\text{--}122^{\circ}\text{E}$ , $30^{\circ}\text{--}42^{\circ}\text{N}$ )	FJ Province ( $115^{\circ}\text{--}122^{\circ}\text{E}$ , $24^{\circ}\text{--}29^{\circ}\text{N}$ )
$\text{SO}_2 [\text{Tg}(\text{SO}_2) \text{ yr}^{-1}]$	16.89	1.61
Anthropogenic	16.88	1.58
Biomass burning	0.01	0.03
$\text{NO} [\text{Tg}(\text{NO}) \text{ yr}^{-1}]$	11.21	1.85
Anthropogenic	11.19	1.81
Biomass burning	0.01	0.03
Biogenic emissions	0.01	0.01
$\text{NH}_3 [\text{Tg}(\text{NH}_3) \text{ yr}^{-1}]$	2.82	0.43
Anthropogenic	2.79	0.37
Biomass burning	0.03	0.06
$\text{BC} [\text{Tg}(\text{C}) \text{ yr}^{-1}]$	0.93	0.13
Anthropogenic	0.92	0.11
Biomass burning	0.01	0.02
$\text{OC} [\text{Tg}(\text{C}) \text{ yr}^{-1}]$	1.54	0.42
Anthropogenic	1.46	0.22
Biomass burning	0.08	0.20
$\text{CO} [\text{Tg}(\text{CO}) \text{ yr}^{-1}]$	91.51	14.23
Anthropogenic	90.04	10.88
Biomass burning	1.38	3.21
Biogenic emissions	0.09	0.14

study periods, the cloud covers were as low as less than 2%; thus, the differences in meteorological conditions and  $\text{PM}_{2.5}$  concentrations between DEF\_ANT\_RAD and DEF\_ANT\_NORAD nearly reflected the aerosol direct radiative effect and first indirect effect, which was referred to as aerosol radiative feedbacks (ARFs) in the context. Third, an additional three sensitivity simulations with aerosol radiative feedbacks turned off were performed to estimate the relative contribution of local emission sources and long-range transport on aerosol concentrations in Xiamen: 1) the anthropogenic emissions in Fujian Province were eliminated (0%FJ\_ANT\_NORAD); 2) the anthropogenic emissions in the YRD region were eliminated (0%YRD\_ANT\_NORAD); and 3) the anthropogenic emissions in the NCP region were eliminated (0%NCP\_ANT\_NORAD). The locations of Fujian and the NCP and YRD regions are shown in Fig. 1d.

### b. Observations

The surface meteorological data were used to evaluate model performances. The data included 1) the land-based observations made every 6 h at eight meteorological stations archived at the National Centers for Environmental Information ([www.ncdc.noaa.gov/data-access/land-based-station-data](http://www.ncdc.noaa.gov/data-access/land-based-station-data)); 2) hourly observations at the Xiamen site of the local meteorological bureau; and 3) hourly wind records from a meteorological buoy deployed in Taiwan Strait, which is affiliated with the Third Institute of Oceanography, State Oceanic

TABLE 3. Experimental design.

Simulation name	Description
DEF_ANT_RAD	Default anthropogenic emissions
DEF_ANT_NORAD	Default anthropogenic emissions with aerosol feedback off
Emission reduction scenarios	
0%FJ_ANT_NORAD	No anthropogenic emissions in FJ Province; otherwise identical to DEF_ANT_NORAD
0%YRD_ANT_NORAD	No anthropogenic emissions in YRD; otherwise identical to DEF_ANT_NORAD
0%NCP_ANT_NORAD	No anthropogenic emissions in NCP; otherwise identical to DEF_ANT_NORAD

Administration of China. The simulated winds in the troposphere were compared with the radiosonde observations from the Integrated Global Radiosonde Archive (IGRA; [www.ncdc.noaa.gov/data-access/weather-balloon/integrated-global-radiosonde-archive](http://www.ncdc.noaa.gov/data-access/weather-balloon/integrated-global-radiosonde-archive)). The radiosonde observations were available on the World Meteorological Organization mandatory pressure levels (e.g., 1000, 925, 850, 500, 400, 300, 250, 200, 150, 100, 70, 50, and 10 hPa) at three local sites, with time resolution of 2 times per day (0000 and 1200 coordinated universal time). The hourly PM<sub>2.5</sub> observations were collected by the China National Environmental Monitoring Centre and contained records for Fujian during winter 2013. Aerosol optical depth (AOD) at a wavelength of 550 nm was retrieved from the level 3 Moderate Resolution Imaging Spectroradiometer (MODIS)/*Aqua* products with a grid resolution of 1° × 1° and used for comparison with the simulated AOD.

### 3. Evaluation of the model performance

The Model Evaluation Tools (MET) toolkit ([www.dtcenter.org/met/users/](http://www.dtcenter.org/met/users/)) has been used to extract variables from WRF-Chem simulations. Details on MET have been previously described in Fast et al. (2011). The evaluation is conducted in terms of spatial distribution (Figs. 2 and 3), multiday and diurnal variations (Figs. S3–S7 in the online supplementary material), and vertical profiles (Fig. 4) for all study periods. The main statistical metrics used for model evaluation include correlation coefficient *R*, mean bias (MB), and root-mean-square error (RMSE). Formulas for these metrics are given in the online supplementary document [Eqs. (S1) and (S2)]. For model evaluation, we define haze days when the observed PM<sub>2.5</sub> exceeds 75 μg m<sup>-3</sup>, and the others are clear days. If not otherwise specified, the model results presented in this section are from the baseline simulation (DEF\_ANT\_RAD), which represents the most comprehensive realization of the different processes in the model.

#### a. Temperature

The spatial distribution of model performance for temperature shows that the model overall reproduces

the temperature pattern in the region, with relatively high temperatures at sites along the coast and relatively low temperatures at sites in the inland of Fujian (Fig. 2a). During 1–24 December, the model simulates hourly temperature with a correlation of 0.87 and an average warmer bias of 0.01°C over nine sites in the region (Table S1a in the online supplementary material). Spatially, the temperature biases are larger along the coast (from -0.85° to 1.38°C; Fig. 2a). The biases might be related to the model resolution of 9 km, which is insufficient to accurately capture the coastal temperature gradient, due to the local-scale atmospheric thermodynamics and dynamics, and inaccurate land use and land cover (e.g., some land areas are modeled as water and vice versa). It is worth noting that cold biases occur at Gaoqi (-0.85°C) and Xiamen (-0.17°C), located in the developed Xiamen Island. Such cold biases are also likely related to unresolved surface properties since the island is experiencing urbanization and the coarse model resolution is not fine enough to resolve small-scale circulations in an urban environment.

The diurnal variations of temperature (Fig. S3) are simulated with a correlation of 0.89 and 0.84 for day and night, respectively (Table S1a), showing a nighttime warm bias (0.29°C) and a daytime cold bias (-0.33°C). The biases are consistent with a previous study in complex terrain due to errors from land use, PBL parameterization, and so on (Massey et al. 2016; Zhang et al. 2013). The model generally captures the multiday variation on both clear and haze days (Fig. S3) except for some underpredictions of -0.94°C on haze days and overpredictions of 0.49°C on clear days (Tables S1b,c). The largest biases occur in daytime during the haze days, with average cold biases of -1.28°C. The large bias during the haze days might be related to too strong a cold surge due to the overestimation of wind speed (Tables S1a–c) and cold biases in the WRF model for winter in China that have been reported by Zhang et al. (2015). Figure 4 compares simulated vertical profiles of temperature with atmospheric radiosonde observations recorded between the ground and 10 hPa. The model can capture the temperature vertical profile well, with

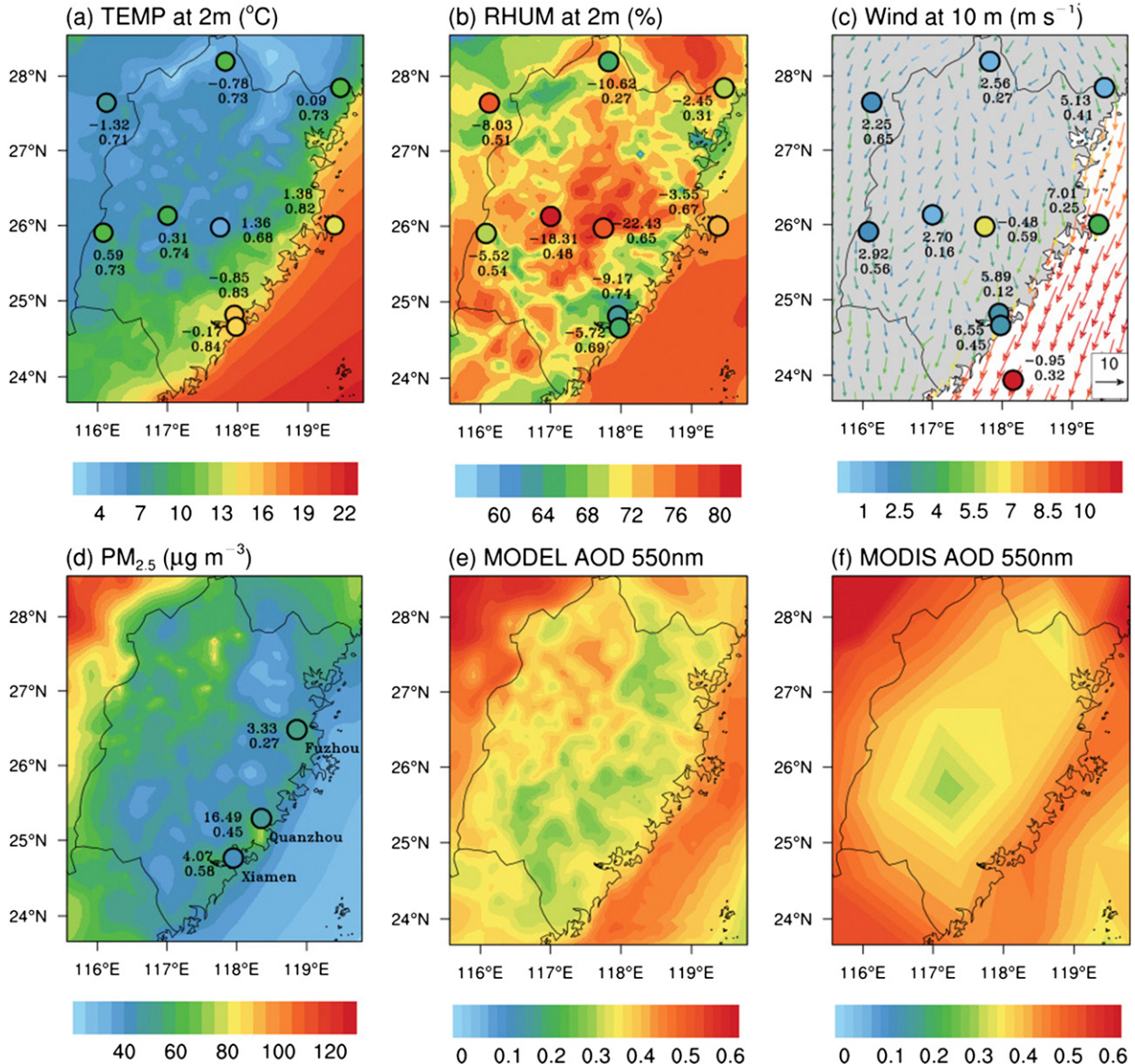


FIG. 2. The mean observed (points) and simulated (color shades) (a) 2-m temperature ( $^{\circ}\text{C}$ ), (b) 2-m relative humidity (%), (c) 10-m wind fields ( $\text{m s}^{-1}$ ), (d) surface-layer PM<sub>2.5</sub> concentrations ( $\mu\text{g m}^{-3}$ ), and 550-nm AOD from the (e) simulation and (f) MODIS in FJ Province in December 2013. The numbers near each site in (a)–(d) denote the model MBs (top number) and correlation coefficients (bottom number) between the simulations and the observations. The numbers in (c) are calculated on the basis of wind speeds. The site names are given in Fig. 3.

large uncertainties that appear in the lower levels reflecting the varying boundary layer meteorological conditions, which require higher model resolution and finer downscale resolution.

#### b. Relative humidity

The spatial distribution of relative humidity is generally captured (Fig. 2b), with correlations greater than 0.5 at most sites except two sites in the north. The maximum bias is  $-22.43\%$  at Jiuxianshan, a 1653-m-high site in the

center of Fujian. The large underestimated biases in the inland might be related to unresolved topographic features in surface drag parameterization and the coarse resolution of the domain. The high topography causes the air to rise, thereby increasing the relative humidity via adiabatic cooling. Thus, the subgrid physical processes may not be well represented because of the smoothed topography used in the model. The multiday variation shows that the largest biases occur during the haze days (Fig. S4), with average drier biases of  $-9.34\%$

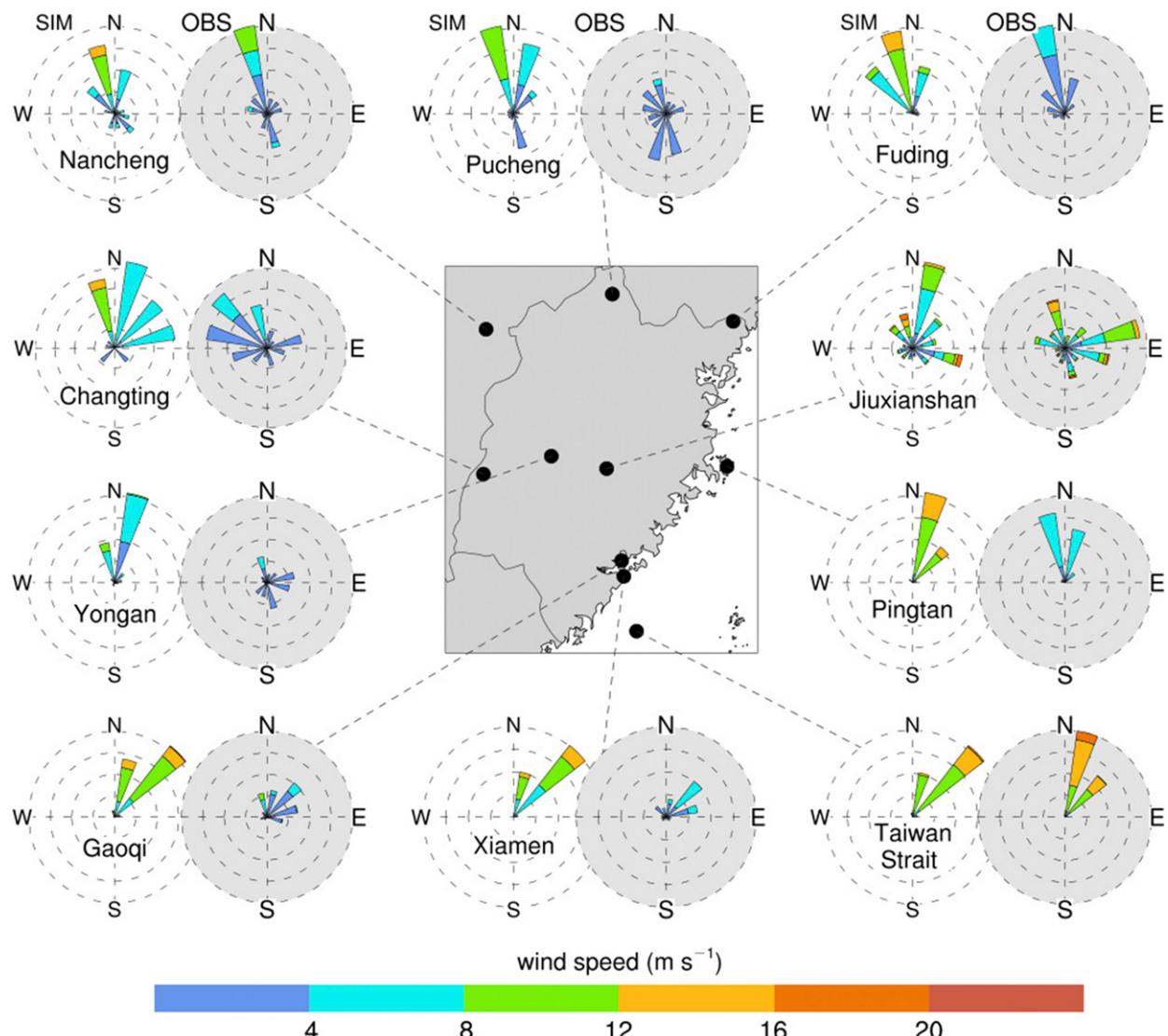


FIG. 3. The 10-m winds ( $\text{m s}^{-1}$ ) from the simulations (SIM; clear circles) and observations (OBS; gray-shaded circles) in FJ Province during 1–24 Dec 2013.

(Table S1b), consistent with the colder bias in temperature.

#### c. Wind

The model systematically overestimates the observed wind speed at most sites (Fig. 2c), overpredicted by  $2.76 \text{ m s}^{-1}$  on average except for the site in the ocean. Wind speed in the narrow Taiwan Strait is high, up to  $11.5 \text{ m s}^{-1}$ , which is underestimated by approximately  $1 \text{ m s}^{-1}$  in the model. Large biases are found in the sites along the coastline, with biases reaching  $5\text{--}7 \text{ m s}^{-1}$  (Fig. 2c and Fig. S5). The WRF-based models systematically overestimated wind speeds in Europe or North America or Asia as has been presented by previous

studies (Vautard et al. 2012; Zhang et al. 2016b). This relatively high wind bias is consistent with the large cold bias in temperature, suggesting too strong wind from the north, which might lead to too strong dilution of air pollutants in the NCP and YRD and rapid transport to the downwind regions. The poor model performance along the coastline may partly result from unresolved land-sea cover (e.g., some water areas are modeled as land and vice versa). The multiday variation shows winds are overestimated by  $3.21 \text{ m s}^{-1}$  on haze days (Table S1b) and  $2.53 \text{ m s}^{-1}$  on clear days (Table S1c).

The comparisons of surface wind directions between the simulations and the observations are shown in Fig. 3. The model captures the prevailing north-northeasterly

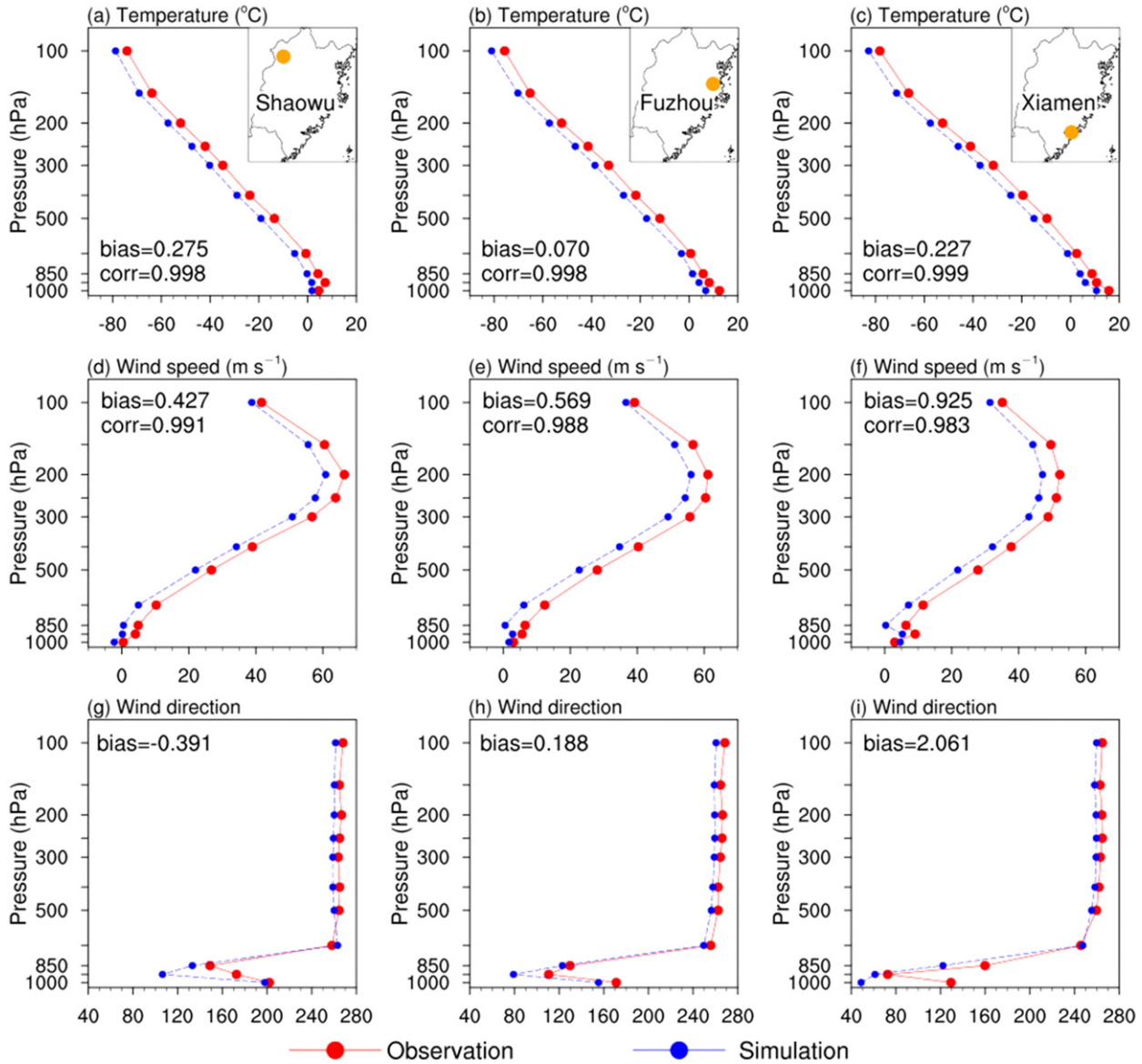


FIG. 4. The mean twice-daily radiosonde-observed (red) and simulated (blue) vertical profiles of (a)–(c) air temperature ( $^{\circ}\text{C}$ ), (d)–(f) wind speed ( $m s^{-1}$ ), and (g)–(i) wind direction (clockwise from the north) at Shaowu, Fuzhou, and Xiamen in FJ Province during 1–24 December 2013. The MB and the correlation coefficient (corr) in the troposphere are also shown. The model results (blue) are interpolated to the pressure levels of the observations and intentionally reduced by 5 units for clarity.

surface winds at the coastal sites (e.g., Fuding, Pingtan, Xiamen; Gaoqi, and in the Taiwan Strait), but the performance is poor in the mountainous area (e.g., Pucheng, Changting, and Yongan). The complex inland topography and heterogeneous surface properties lower the ability of the model to capture subgrid wind structures. Wind profiles show wind biases are limited in the PBL and very small in the upper troposphere (Fig. 4). The diurnal variation of wind vectors at 10-m height are shown in Figs. S5 and S6. The simulated winds are higher than the observations at most sites, especially at the

nighttime. The nighttime wind bias is larger than in the daytime (Table S1a) because of the well-known inability of meteorological models to accurately simulate nocturnal turbulent mixing near the surface (Ngan et al. 2013).

#### d. $PM_{2.5}$

Spatially, the model systematically overestimates the observed  $PM_{2.5}$  at all sites, with an average of  $7.92 \mu\text{g m}^{-3}$  (Table S1a), especially in the Quanzhou site, where it is about  $16.49 \mu\text{g m}^{-3}$  (Fig. 2d). The large

model errors occur in Quanzhou, which might be related to the fact that there is a relatively strong concentration gradient near the city that is not captured because of the resolution error. The multiday and diurnal variations of the observed and simulated PM<sub>2.5</sub> (Fig. S7) show the model-simulated hourly PM<sub>2.5</sub> with a temporal correlation of 0.27 at Fuzhou, 0.45 at Quanzhou, and 0.58 at Xiamen. The largest overestimation is found during haze days at nighttime, up to 24.58  $\mu\text{g m}^{-3}$ , consistent with the largest colder temperature, drier humidity, and higher wind speed biases. The model overestimation during the severe winter haze episodes is in contrast to underestimation reported in previous studies focusing on haze in the NCP (Zhang et al. 2015). Possible sources for the overestimated PM<sub>2.5</sub> concentrations might be related to 1) too strong transport of pollutants induced by the cold surge or 2) unresolved wind and temperature gradients along coastal regions as mentioned in sections 3a–c.

#### e. AOD

The evaluation of the simulated and observed AOD over China clearly shows that the regional-scale AOD simulations have large underpredictions in northern China (Fig. S8). The model fails to reproduce the extremely high sulfate concentrations in wintertime haze because of lack of sulfate formations via heterogeneous reactions catalyzed by transition metal ions (Alexander et al. 2009; X. Huang et al. 2014; Zheng et al. 2015; Chen et al. 2016; Dong et al. 2016) and in aqueous oxidation as coexistence of NO<sub>2</sub> in high-humidity conditions (He et al. 2014; G. Wang et al. 2016). Nevertheless, the model successfully reproduced the AOD pattern in Fujian (Figs. 2e,f), with a model bias of −0.05 (−11.6%), which is lower than the upper-limit value of uncertainty of MODIS AOD (30%, assuming AOD = 0.3 in the uncertainty envelope  $0.05 \pm 0.15 \times \text{AOD}$  over land; Remer et al. 2005). The AOD bias is likely related to 1) local emission uncertainties; 2) the underpredicted PM<sub>2.5</sub> concentrations over northern China and, hence, fewer aerosols transported into Fujian; 3) the uncertainties included in the lateral boundaries obtained from MOZART, which has been suggested to be likely too high in the free troposphere (Fast et al. 2014) and thus might contribute to errors in simulated AOD; 4) the lack of SOAs in the simulations because the SOAs might be absorbing at the near-UV range; 5) the model error due to four size bins of particles in simulation; 6) the model bias in relative humidity, as mentioned in section 3b, which affects aerosol hygroscopic growth; and 7) the possible bias in the retrieval algorithm used in deriving MODIS monthly AOD (Kaufman et al. 2005).

In general, despite the model biases in magnitudes, the performance of the WRF-Chem model reproduces the geographical patterns and the variations of meteorological parameters and PM<sub>2.5</sub> in Fujian. It is therefore suited for application in determining the impact of meteorological conditions, aerosol radiative feedbacks, and emission reduction scenarios on PM<sub>2.5</sub> concentrations.

### 4. Linkage between meteorological conditions and PM<sub>2.5</sub>

#### a. Airmass transport pathways to Xiamen

In comparison with northern China, the anthropogenic emissions in Fujian are relatively low (Table 2 and Fig. S1), and PM<sub>2.5</sub> loading is also low (Fig. 2d). Air quality in Fujian is impacted by the emissions from various sources both from local human activities and long-range transport, the relative contributions of which are related to atmospheric circulation. To identify the transport pathways and potential airmass origins, cluster analysis is applied to the 5-day backward trajectories calculated by the HYSPLIT\_4 model (Draxler and Hess 1998), and four potential transport routes are identified (Fig. 1c): 9% of air masses are from the pathway related to the cold surge (cluster CS), 37% are from the northeast route (cluster NE), 14% are local air masses (cluster LC), and 40% originate from the ocean, named ocean routes (cluster OE).

#### b. Meteorological patterns and PM<sub>2.5</sub>

The time series variation of PM<sub>2.5</sub> concentrations and airmass transport pathways are shown in Fig. 5a. One can see that PM<sub>2.5</sub> concentrations are mostly controlled by the four transport pathways. Specifically, 1) episode A (on 2–3 December) has a moderately high PM<sub>2.5</sub> concentration, which is related to air masses in cluster NE; 2) haze episode C (9–10 December) has the highest PM<sub>2.5</sub> concentration: when air masses arrive at Xiamen via two pathways, one route is cluster NE similar to that during episode A, and the other is cluster CS that features a long mean trajectory, indicating fast southward propagation of air masses induced by the cold surge; 3) clean episode B (on 6–8 December) is related to air masses originating from the ocean (cluster OE); and 4) haze episode P1 (the night of 4–5 December) and PM<sub>2.5</sub> peak P2 (the night of 8–9 December) are related to local air masses (cluster LC), when airmass trajectories are relatively short under calm weather conditions.

During episode A, there are southerly winds in the north and west of Fujian Province, which prevent the southward transport of inland pollutants from invading Xiamen. Instead, the northeasterly winds in the coastal regions coming from the YRD region transport the

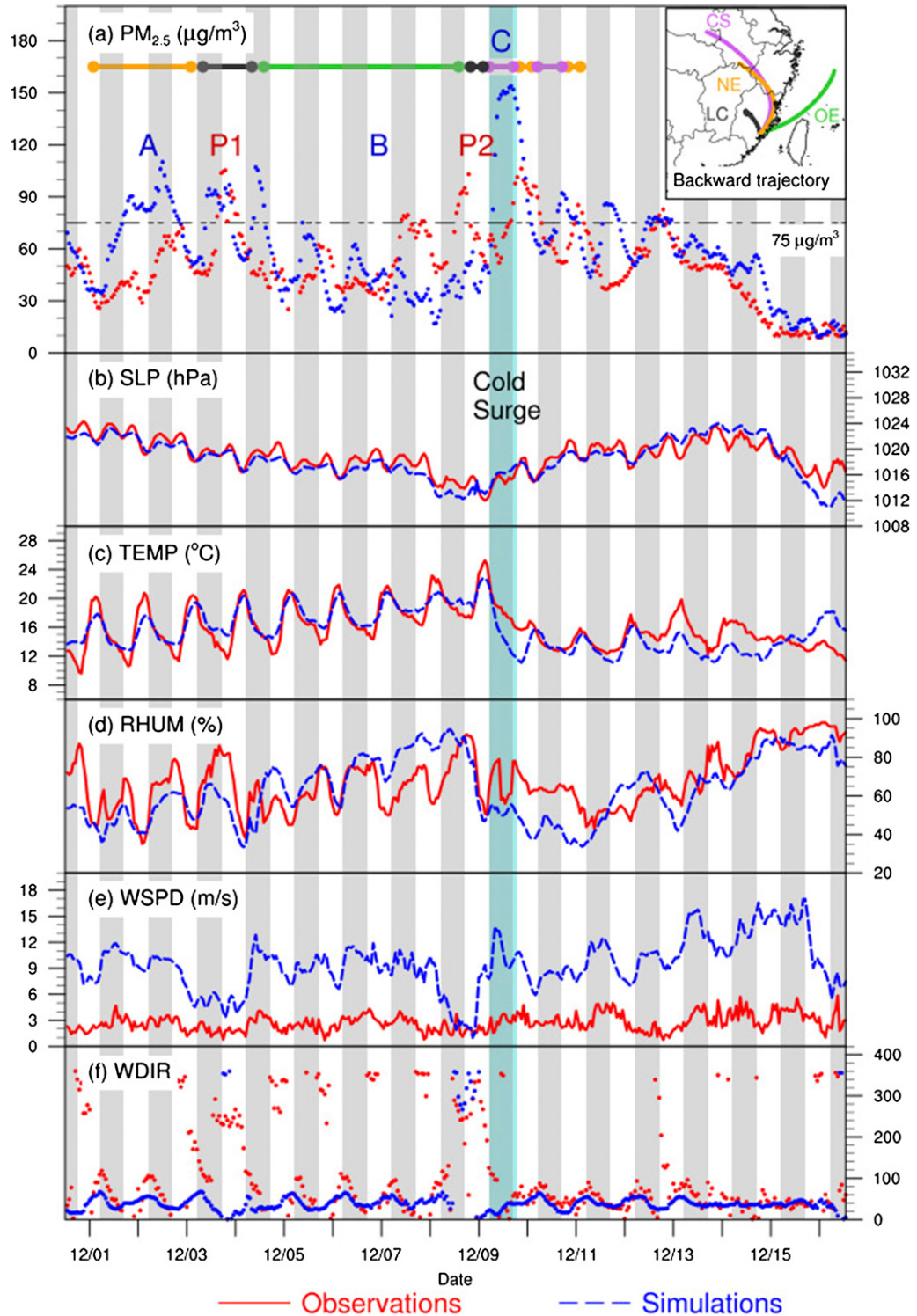


FIG. 5. (a) Observed (red) and simulated (blue) hourly surface-layer PM<sub>2.5</sub> concentrations ( $\mu\text{g m}^{-3}$ ) in Xiamen. The inset figure shows the airmass transport pathways; the dashed line in the middle is the 24-h limit of the Chinese ambient air quality grade II standard (75  $\mu\text{g m}^{-3}$ ). (b) SLP (hPa), (c) 2-m air temperature (TEMP;  $^{\circ}\text{C}$ ), (d) 2-m humidity (RHUM; %), (e) 10-m wind speed (WSPD;  $\text{m s}^{-1}$ ), and (f) wind direction (WDIR; clockwise from the north in degrees) on 1–16 Dec 2013. The gray bars indicate the nighttime from 1800 to 0600 LCT. Tick marks on the x axis indicate 1200 LCT.

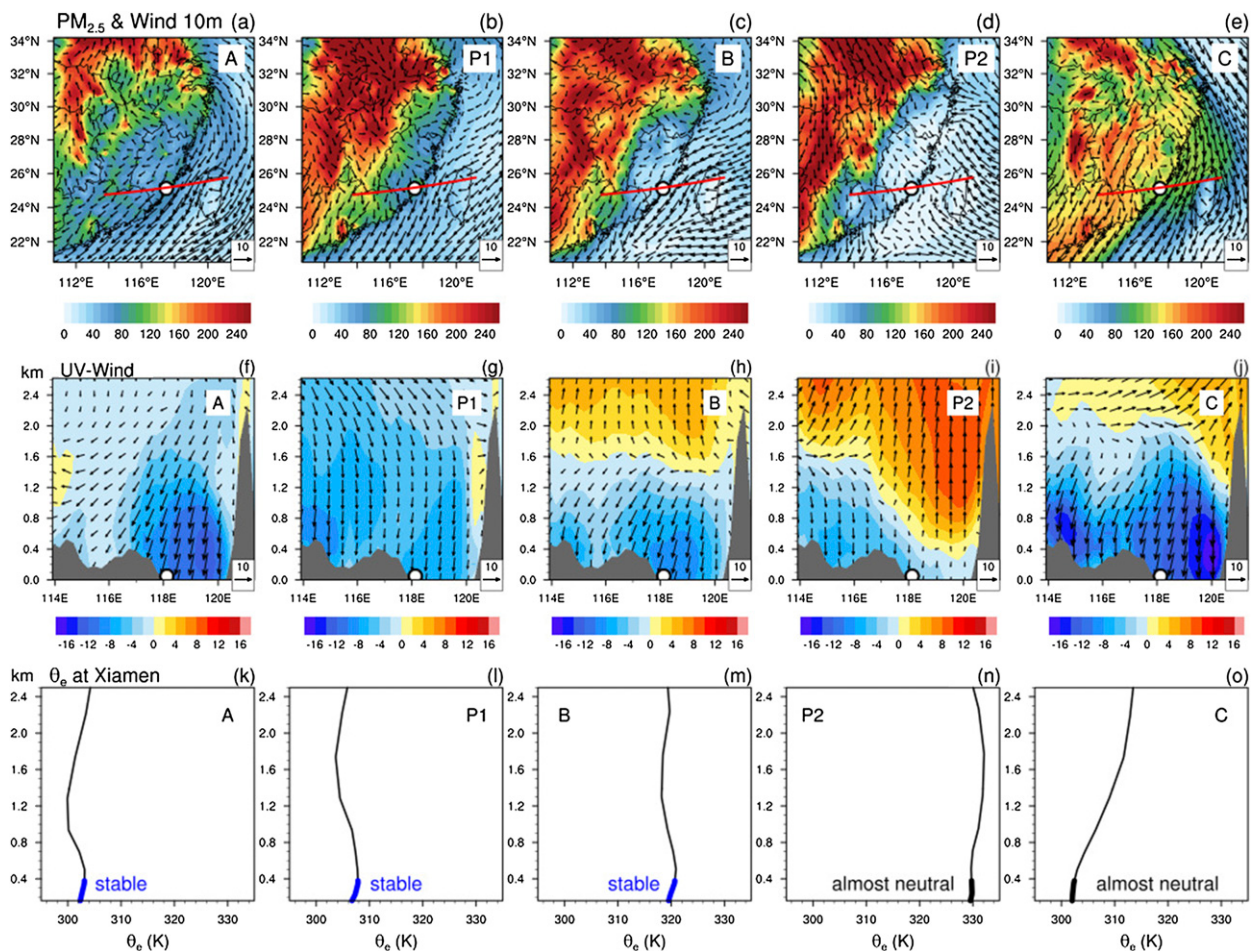


FIG. 6. Simulated (a)–(e) mean surface-layer PM<sub>2.5</sub> and 10-m wind vectors, (f)–(j) wind vectors and  $v$  wind components (color shades) at cross sections that are defined along the red lines as shown in (a)–(e), and (k)–(o) the vertical profiles of equivalent potential temperatures  $\theta_e$  for each episode. The positive (negative)  $v$  wind components denote northerly (southerly) winds. The units are micrograms per meter cubed for PM<sub>2.5</sub>, meters per second for winds, and kelvins for equivalent potential temperature.

inland pollutants to the south (Fig. 6a). The strong tangential wind in the coastal zone converges with the inland side of the low wind (Fig. 6f), accompanied with a stable weather condition in Xiamen (Fig. 6k), which enables the accumulation of pollutants in Xiamen. In addition, when comparing the fluxes at the beginning of episode A (at night on 1 December; Fig. 7a) with the fluxes at the periods when PM<sub>2.5</sub> concentrations were high (at night on 2 December; Fig. 7b), it is seen that the changes in fluxes as shown in Fig. 7c indicate a maximum increase in Xiamen. This suggests the increase in PM<sub>2.5</sub> concentrations is related to the increase in the transport of air pollutants from the YRD that then accumulate in Xiamen. The simulated PM<sub>2.5</sub> concentrations are higher, with a factor of 2, than the observations (Table 4). This might be related to overestimated wind speeds, which induce too strong transport from the polluted YRD into the study region.

During episode P1, winds are relatively low, as shown in wind patterns at the surface (Fig. 6b) and in the cross section (Fig. 6g). The atmosphere is stable below 500 m over Xiamen (Fig. 6l). The local air temperature and humidity have nearly identical diurnal variations with similar maximums and minimums on multiple days (Figs. 5c,d) and with low wind speeds (roughly  $4 \text{ m s}^{-1}$ ), and the air masses are of local origin as predicted by the backward trajectory analysis. Under these conditions, the model and the observation agree with high PM<sub>2.5</sub> concentrations (Table 4). The PM<sub>2.5</sub> concentrations gradually increase to approximately  $110 \mu\text{g m}^{-3}$  by 1200 local time (LCT) 4 December. This suggests that the high PM<sub>2.5</sub> concentrations on 3–4 December are likely related to the accumulation of pollutants by stagnant air.

During 5–8 December, strong easterly winds from the ocean bring relatively clean air to the region (cluster

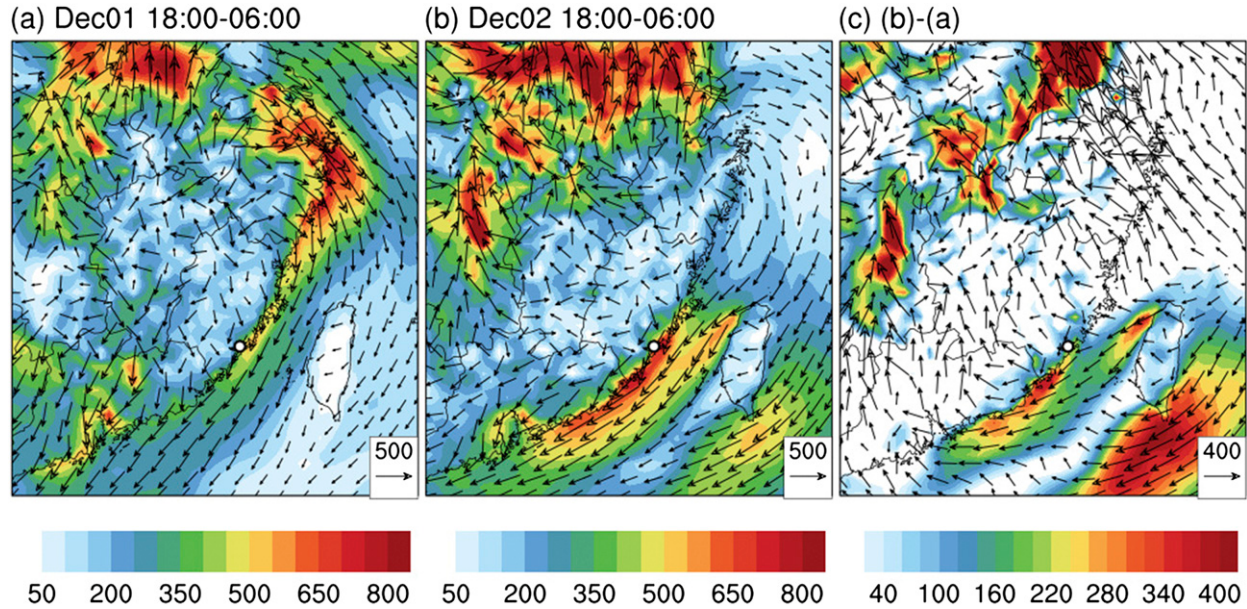


FIG. 7. The simulated surface-layer  $\text{PM}_{2.5}$  flux vectors (i.e., 10-m wind weighted by surface-layer  $\text{PM}_{2.5}$  concentrations) and their magnitudes (color shades;  $\mu\text{g m}^{-2}\text{s}^{-1}$ ) (a) at night on 1 Dec 2013 (the first night of episode A), showing a strong outflow flux of air pollutants from the YRD region; (b) at night on 2 Dec (the second nights of episode A), showing a maximum flux at the coastline ranging from Xiamen to the PRD regions; and (c) their differences, showing the stronger landward components, incurring a maximum flux at the coastline ranging from Xiamen to the PRD region.

OE), lowering  $\text{PM}_{2.5}$  levels (clear days during episode B; Fig. 6c). Noticeably, wind patterns in the cross section show a wind shift to the south above 850 hPa (1.5 km), which is different from the northeasterly winds at the surface (Fig. 6h), indicating a transition of the atmospheric circulation. After that, surface winds shift to the east, which is almost perpendicular to Taiwan, leaving the region to the west of Taiwan with light winds (Fig. 6d). The southerly winds in the upper air become

stronger and propagate to the surface (Fig. 6i), resulting in weak 10-m winds in Xiamen, which induce the accumulation of pollutants and generate a small  $\text{PM}_{2.5}$  peak (P2) during the night when the PBL is low.

The simulated maximum  $\text{PM}_{2.5}$  concentration appears on 9–10 December when a cold surge breaks out. There is a cyclonic anomaly at 850 hPa over the Korean Peninsula, which generates strong northerly winds over mainland China (Fig. S9). Locally, the surface air

TABLE 4. Observed and simulated surface-layer  $\text{PM}_{2.5}$  concentrations, 10-m wind speed, 2-m relative humidity, SLPs, and 2-m air temperatures in Xiamen during the analyzed episodes.

	$\text{PM}_{2.5}$ ( $\mu\text{g m}^{-3}$ )	10-m wind speed ( $\text{m s}^{-1}$ )	2-m relative humidity (%)	SLP (hPa)	2-m air temperature ( $^{\circ}\text{C}$ )
Episode A, cluster NE, from 0800 LCT 2 Dec to 0000 LCT 3 Dec					
Observations	43.24	2.61	53.47	1021.48	16.60
Simulations	88.65	9.69	47.15	1020.99	15.46
Episode P1, cluster LC, from 0100 LCT 4 Dec to 0000 LCT 5 Dec					
Observations	85.64	1.65	78.42	1019.60	13.68
Simulations	85.82	5.07	56.20	1019.35	15.80
Episode B, cluster OE, from 1200 LCT 5 Dec to 1700 LCT 8 Dec					
Observations	49.77	2.58	63.50	1017.72	18.12
Simulations	41.01	9.25	74.70	1016.70	18.41
Episode P2, cluster LC, from 1800 LCT 8 Dec to 0800 LCT 9 Dec					
Observations	78.01	2.07	81.80	1014.73	18.48
Simulations	40.92	3.32	88.98	1012.89	19.56
Episode C, cluster CS, from 1900 LCT 9 Dec to 0800 LCT 10 Dec					
Observations	71.86	3.02	68.86	1015.67	17.66
Simulations	139.89	10.98	52.17	1016.59	14.17

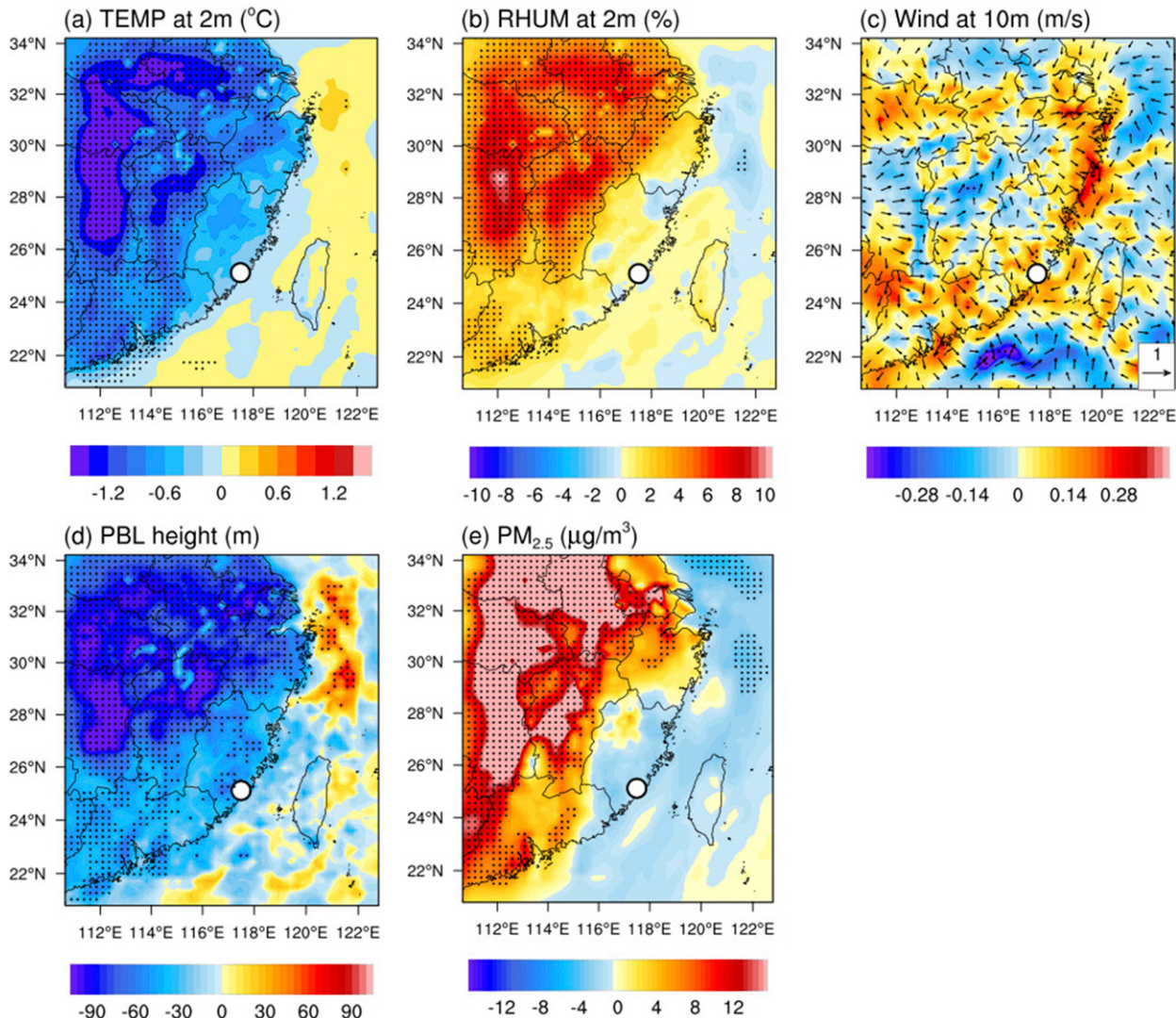


FIG. 8. Simulated ARFs (DEF\_ANT\_RAD minus DEF\_ANT\_NORAD) to (a) 2-m air temperature ( $^{\circ}$ C), (b) relative humidity (%), (c) 10-m wind speed ( $m s^{-1}$ ), (d) PBL height (m), and (e) PM<sub>2.5</sub> ( $\mu g m^{-3}$ ) for 1–14 Dec 2013 in southeastern China. The dotted areas have changes in magnitude that are statistically different at a significance level of 0.05. The changes in 10-m winds are almost insignificant everywhere.

temperature in Xiamen dropped by 8 $^{\circ}$ C over 12 h (25.2 $^{\circ}$ C at 0600 LCT to 17.2 $^{\circ}$ C at 1800 LCT 9 December); the ambient humidity decreased from 89% to 63%; the sea level pressure (SLP) increased by nearly 10 hPa; and the north-northeast prevailing winds had high speeds of 8–10  $m s^{-1}$  (Figs. 5b–f). The southward propagation of the cold surge induces the northern particulates to spread to the southeast region of China, and then the pollutants are divided into two branches in the northwest of Fujian because of the relatively high terrain (Fig. 6e). A few pollutants flow across the terrain and invade Fujian, triggered by the cold surge. More pollutants flow to the east and then turn to the southwest because of forcing by the northeast prevailing winds

over the coastal and ocean regions. The northern continental outflowing pollutants are transported to the south along the coastline and enter the coastal regions in Fujian. Extremely high PM<sub>2.5</sub> concentrations are observed in Xiamen, reaching hazardous levels, with average PM<sub>2.5</sub> concentrations up to 150  $\mu g m^{-3}$  when a cold surge approaches.

In summary, high PM<sub>2.5</sub> concentrations in Xiamen are modulated by atmospheric patterns that either allow pollutants to accumulate or enable external pollutants to impinge into the region. It is worth noting that the highest mean PM<sub>2.5</sub> concentration in Xiamen is associated with the cold surge featuring a cyclonic anomaly over the Korean Peninsula (Figs. S9b–f). This suggests

TABLE 5. ARFs (DEF\_ANT\_RAD minus DEF\_ANT\_NORAD) to PBL height, 10-m wind speeds, 2-m relative humidity, SLPs, 2-m air temperatures, and surface-layer PM<sub>2.5</sub> concentrations in Beijing (domain 1), Hefei (domain 2), and Xiamen (domain 3) on 1–14 Dec 2013.

Site	PM <sub>2.5</sub> ( $\mu\text{g m}^{-3}$ )	PBL height (m)	10-m wind speed ( $\text{m s}^{-1}$ )	2-m relative humidity (%)	SLP (hPa)	2-m air temperature (°C)
Beijing	+13.62	-49.22	-0.07	+1.69	+0.09	-0.54
	+7.46%	-22.36%	-2.08%	+4.17%	+0.01%	-64.25%
Hefei	+32.49	-84.10	-0.05	+6.57	+0.10	-1.38
	+10.26%	-43.31%	-1.81%	+10.50%	+0.01%	-27.20%
Xiamen	-1.91	-27.55	+0.05	-0.37	-0.03	-0.18
	-3.14%	-4.68%	+0.70%	-0.55%	-0.00%	-1.03%

that a cyclonic anomaly over the Korean Peninsula might be a potential indicator for predicting potential high-PM events in winter in Fujian Province or other coastal southeastern regions in China.

## 5. ARFs

After comparing the simulations with aerosol feedbacks turned on (DEF\_ANT\_RAD) and off (DEF\_ANT\_NORAD) in the WRF-Chem model, the results (DEF\_ANT\_RAD–DEF\_ANT\_NORAD; Figs. 8a–d) suggest that ARFs in the southeastern coastal region of Fujian Province are much smaller than the effects that occur in inland China, where they play a significant role in altering meteorological parameters (Fig. S10). ARFs induce a cooler 2-m air temperature with a mean of  $-0.96^\circ\text{C}$  and a lowered PBL height of  $-69.7\text{ m}$  over the regions that have statistically significant changes ( $p < 0.05$ ) in eastern China ( $20^\circ\text{--}45^\circ\text{N}$ ,  $100^\circ\text{--}125^\circ\text{E}$ ). It is interesting to note that ARFs increase PM<sub>2.5</sub> concentrations in inland China, as shown in Fig. S10 and suggested in previous studies (Gao et al. 2015; Zhang et al. 2015), whereas negative changes in PM<sub>2.5</sub> concentrations due to ARFs are found in Fujian Province (Fig. 8e).

Table 5 summarizes the response of meteorological parameters and PM<sub>2.5</sub> to ARFs in typical inland cities—Beijing, in the NCP, Hefei in the YRD region, and Xiamen in southeastern coastal China—along the cross section shown in Fig. 1d. Figure 9 shows the multiday and diurnal variation in changes of PM<sub>2.5</sub> concentrations. During 1–14 December, ARFs induced a cooler temperature and lower PBL height at the three cities. ARFs increased PM<sub>2.5</sub> concentrations by up to 7.46% ( $13.62 \mu\text{g m}^{-3}$ ) and 10.26% ( $32.49 \mu\text{g m}^{-3}$ ) in Beijing and Hefei, respectively, but decreased by 3.14% ( $-1.91 \mu\text{g m}^{-3}$ ) in Xiamen. This indicates that PM<sub>2.5</sub> increases in Beijing and Heifei are associated with the PBL height reduction (Figs. 9a,c), which is in line with previous studies focused on the NCP (Gao et al. 2015; Zhang et al. 2015), whereas changes in PM<sub>2.5</sub> concentrations are not related to changes in PBL in Xiamen

(Fig. 9e), indicating that the mechanisms modulating changes in PM<sub>2.5</sub> in Xiamen might be different from that in Beijing and Hefei.

The multiday variations of PM<sub>2.5</sub> due to ARFs in Xiamen (Fig. 9f) show that ARFs induce both positive and negative changes in PM<sub>2.5</sub> concentrations. Positive changes occur during episodes P1 and P2 when the PM<sub>2.5</sub> peaks are related to local accumulation of pollutants under short periods of calm weather conditions. The PBL height is significantly decreased ( $-150\text{ m}$ ) during episode P1, and the wind speed is significantly decreased ( $-0.28 \text{ m s}^{-1}$ ) during the P2 period, which increases the local pollutants, respectively (Fig. 10). ARFs' impacts in the two episodes are basically consistent with that in Beijing and Hefei.

It is interesting to note that negative effects of ARFs on PM<sub>2.5</sub> concentrations are found during episodes A and C and clean episode B, when PM<sub>2.5</sub> concentrations were affected by air masses transported from long distances via the CS, NE, and OE pathways. During episode A, ARFs induce northwesterly wind anomalies at Xiamen (Fig. S11a), which can push away the PM<sub>2.5</sub> convergence zone (Fig. 7c) leaving the coastline and decrease PM<sub>2.5</sub> in Xiamen. The changes in 10-m winds are not significant, resulting in limited and short-term decreases in PM<sub>2.5</sub> concentrations. During clean episode B, ARFs induce stronger southeasterly wind anomalies (Fig. 10c), bringing relatively clean air from the ocean (Fig. S11c). Meanwhile, ARFs increase the local PBL height, which helps the dispersion of pollutants and further lowers PM<sub>2.5</sub> concentrations (Fig. 10b). During episode C, when there is a cold surge on 9–10 December, the cross section of ARFs indicates that the reduced PBL height further enhances the blocking of northern particulates crossing the terrain (Fig. 11b).

## 6. Effects of emission reduction scenarios on PM<sub>2.5</sub> in Fujian

On 8 December 2014, the Xiamen municipal government declared air quality control targets for 2014–20

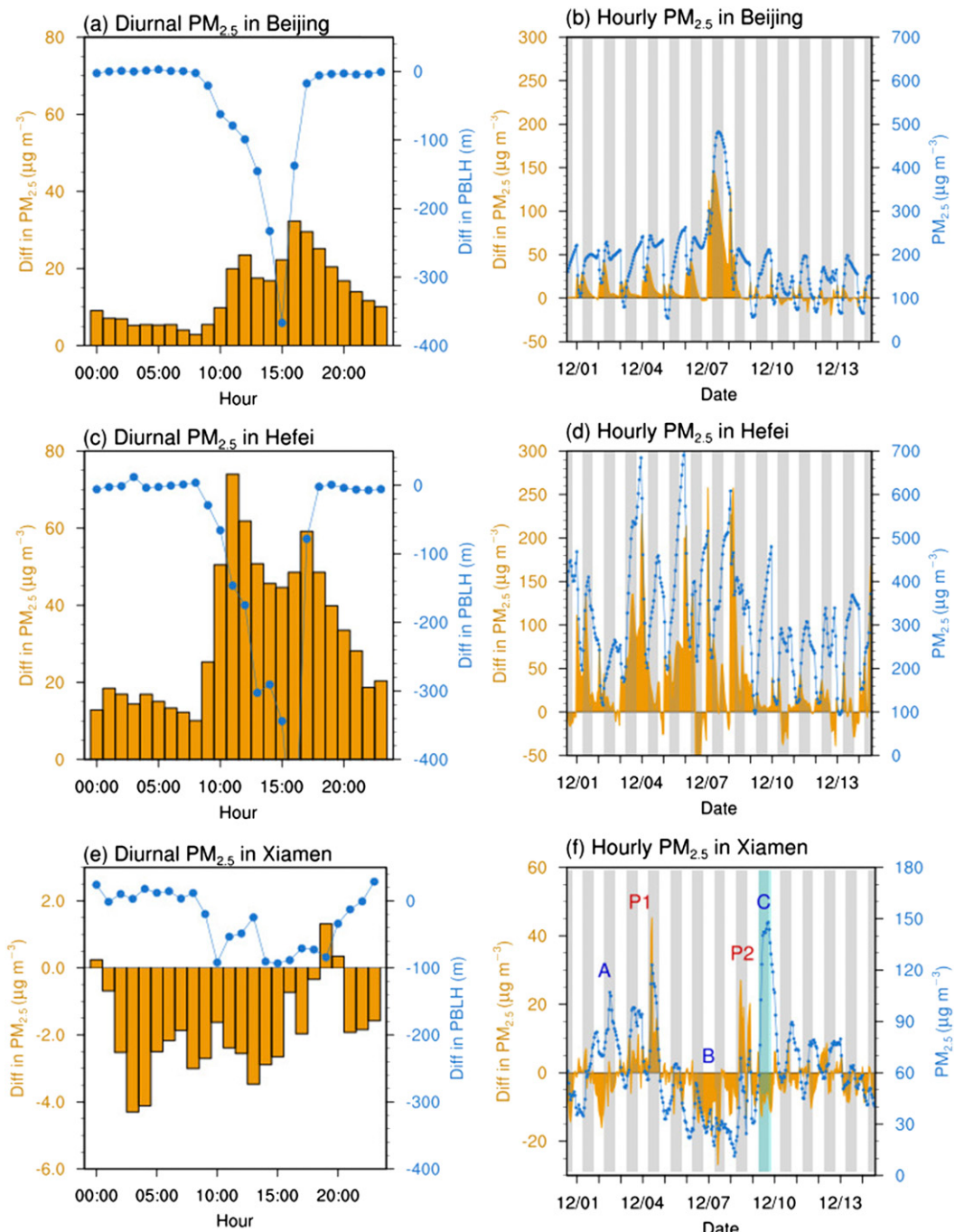


FIG. 9. (left) Diurnal and (right) hourly changes in surface-layer PM<sub>2.5</sub> ( $\mu\text{g m}^{-3}$ ) and PBL height due to ARFs (DEF\_ANT\_RAD minus DEF\_ANT\_NORAD) in (a),(b) Beijing, (c),(d) Hefei, and (e),(f) Xiamen on 1–14 Dec 2013. The gray bars in the right panels indicate the nighttime from 1800 to 0600 LCT. The cold surge reached the FJ Province on the night of 9 Dec.

and intended to keep the annual PM<sub>2.5</sub> concentrations below 55  $\mu\text{g m}^{-3}$ . The potential for exceeding the PM<sub>2.5</sub> standards is ultimately determined by emissions. Air quality in Fujian Province is affected by various emission sources, both internal and external. To

provide guidance for decision-makers, three sensitivity simulations are conducted to quantify how the air quality in terms of PM<sub>2.5</sub> in Xiamen is affected by emission reductions by two major external contributing sources (the NCP and YRD regions) and an

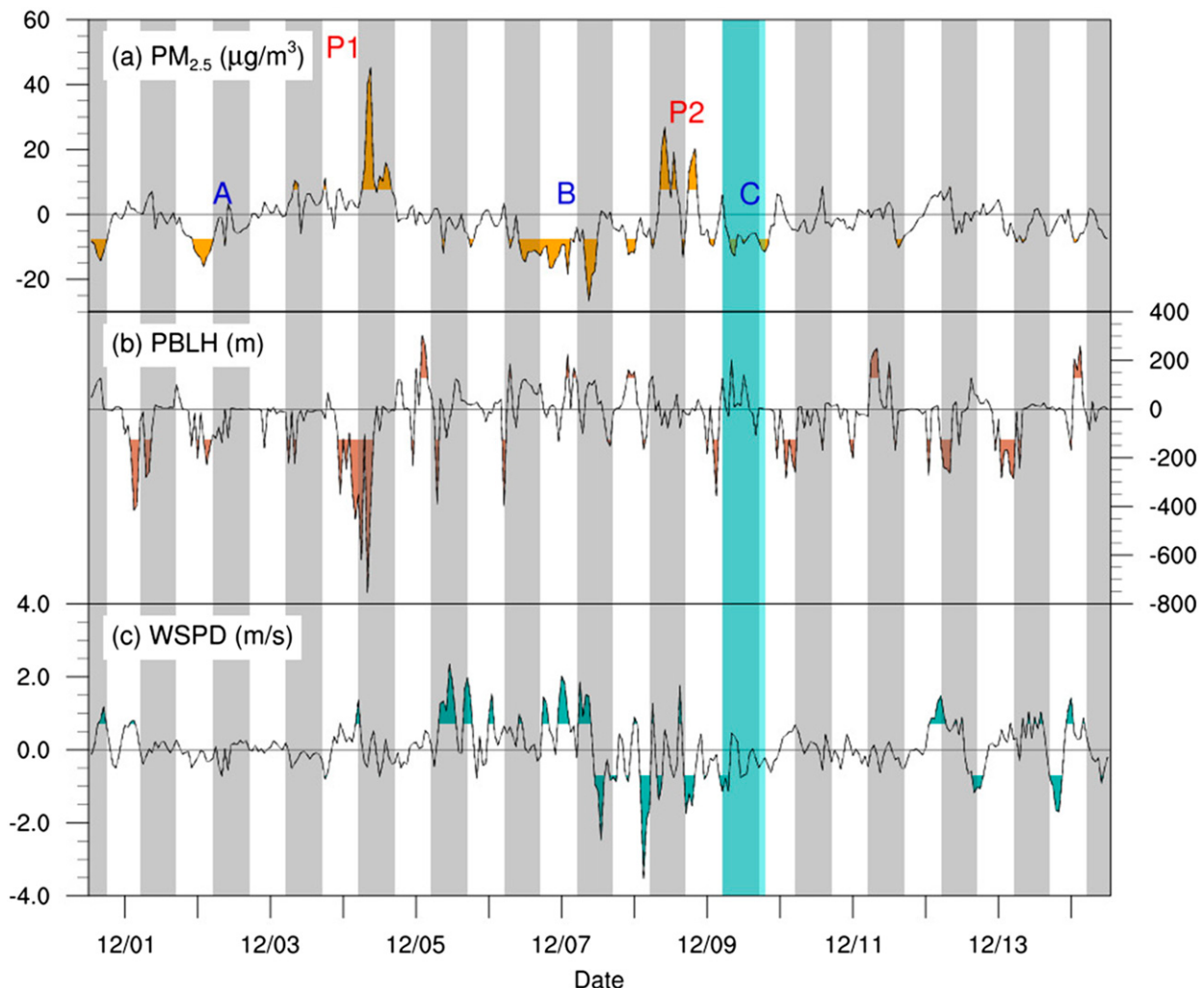


FIG. 10. Simulated ARFs (DEF\_ANT\_RAD minus DEF\_ANT\_NORAD) to (a) surface-layer PM<sub>2.5</sub> ( $\mu\text{g m}^{-3}$ ), (b) PBL height (m), and (c) 10-m wind speeds ( $\text{m s}^{-1}$ ) in Xiamen. The changes that are larger than 1 standard deviation of the physical variable variations on 1–14 Dec are regarded as significant and are marked with colors.

internal source (Fujian; Fig. 12). The scenarios are presented in Table 3. As anticipated, the sums of PM<sub>2.5</sub> concentrations from individual emission sources are not equal to the total concentration. The differences are represented as residual components in Fig. 12. Large residuals in the current sensitivity simulations are likely related to the nonlinear chemical productions due to different precursors' concentrations in each emission reduction scenario. Further research studying chemical species formation in these cases and a sensitivity test for each sector's emission reductions is recommended.

Nevertheless, the multiday PM<sub>2.5</sub> variations in Xiamen (Fig. 12) show that the contribution of external and internal sources change under different atmospheric circulation patterns. The PM<sub>2.5</sub> concentrations are more

sensitive to emission reductions in Fujian under stagnant weather conditions. There are 41.6% of PM<sub>2.5</sub> associated with Fujian emissions, and only 7.4% is from YRD, and 5.6% is from NCP during haze episode P1 (the night of 4–5 December), while during 9–10 December, PM<sub>2.5</sub> from Fujian emissions decreases to 8.8%, whereas those from the YRD and NCP emissions increase to 16.6% and 12.1%, respectively. Therefore, PM<sub>2.5</sub> levels are strongly influenced by emissions in the two major external sources (NCP and YRD), especially during cold surges when plume impingements are favored with northerly winds so that external emissions contribute mostly to the extreme peak concentrations. Since a weak winter monsoon and a decline in cold surges have been shown for the recent years (Niu et al. 2010; Qu et al. 2015) because of global climate change, it is likely that

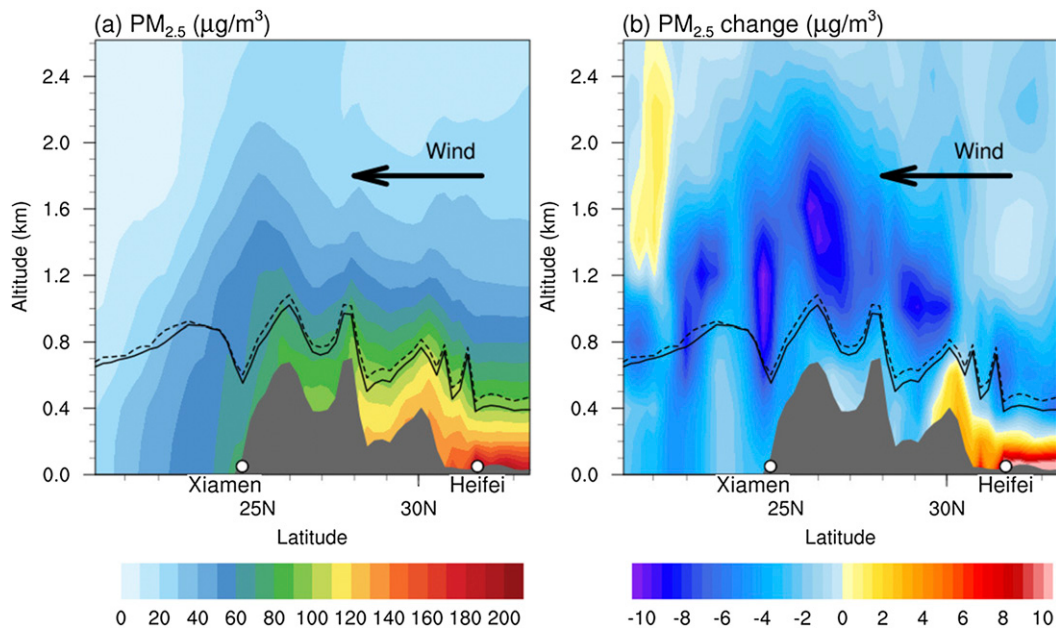


FIG. 11. (a) The baseline PM<sub>2.5</sub> concentrations (in DEF\_ANT\_RAD) and (b) the changes ( $\mu\text{g m}^{-3}$ ) due to ARFs (DEF\_ANT\_RAD minus DEF\_ANT\_NORAD) along the cross section between Xiamen and Beijing (Fig. 1d) during the cold-surge episode on 9–10 Dec. Topography is represented in gray. Also shown are the simulated PBL heights with (solid line) and without (dashed line) ARFs.

air quality in Xiamen is more related to local emissions, and the municipal government thus should implement more aggressive emission reduction policies in addition to the nationwide reduction strategies. Cooperation with external emission reduction is also required to mitigate the extreme haze associated with long-range pollutant transport to Xiamen.

## 7. Summary

We applied the WRF-Chem model to investigate the factors that affected the haze events in December 2013 in Fujian Province, particularly focusing on the meteorological conditions, emissions, and aerosol radiative feedbacks. The model reasonably reproduces the overall meteorological conditions and PM<sub>2.5</sub> concentrations in Fujian. The main findings of this study are as follows:

- 1) The long-range transport played an important role in the extremely high PM<sub>2.5</sub> concentrations during winter in Xiamen. On the night of 9–10 December, the maximum PM<sub>2.5</sub> concentrations in Xiamen were a result of the southward-propagating cold surge transporting high levels of pollutants from the north to the southeastern coastal region. The highest PM<sub>2.5</sub> concentrations were very sensitive to emission reductions in the YRD and NCP, which greatly diminished the PM<sub>2.5</sub> level to 16.6%

and 12.1%, respectively, based on the model sensitivity test.

- 2) High-PM<sub>2.5</sub> events occurred under different meteorological conditions, either due to calm weather conditions (e.g., episodes P1 and P2) or southward transport of the pollutants along the coastline from inland China (e.g., episodes A and C), whereas air masses from the ocean acted as a cleaning agent, leading to low PM<sub>2.5</sub> concentrations (e.g., clean episode B).
- 3) Aerosol feedbacks were unlikely to increase PM<sub>2.5</sub> concentrations in Fujian Province in contrast to the significant aerosol positive feedbacks to PM<sub>2.5</sub> concentrations in inland China. Although positive feedbacks on PM<sub>2.5</sub> concentrations appeared in the short term (e.g., episodes P1 and P2), under the calm weather conditions associated with the lower PBL height-enhanced PM accumulation in Xiamen, ARFs often decreased PM<sub>2.5</sub> concentrations (e.g., the A, B, and C periods) as a result of the offshore wind anomalies induced by ARFs, which push away the coastal PM<sub>2.5</sub> convergence zone originating from the YRD region, lower PBL height over inland China, and hence decrease particles crossing the high terrain in the north of Fujian Province or bring additional clean air from the ocean. This indicates the ARFs were unlikely to strengthen haze intensity in southeastern coastal China as occurs in northern China.

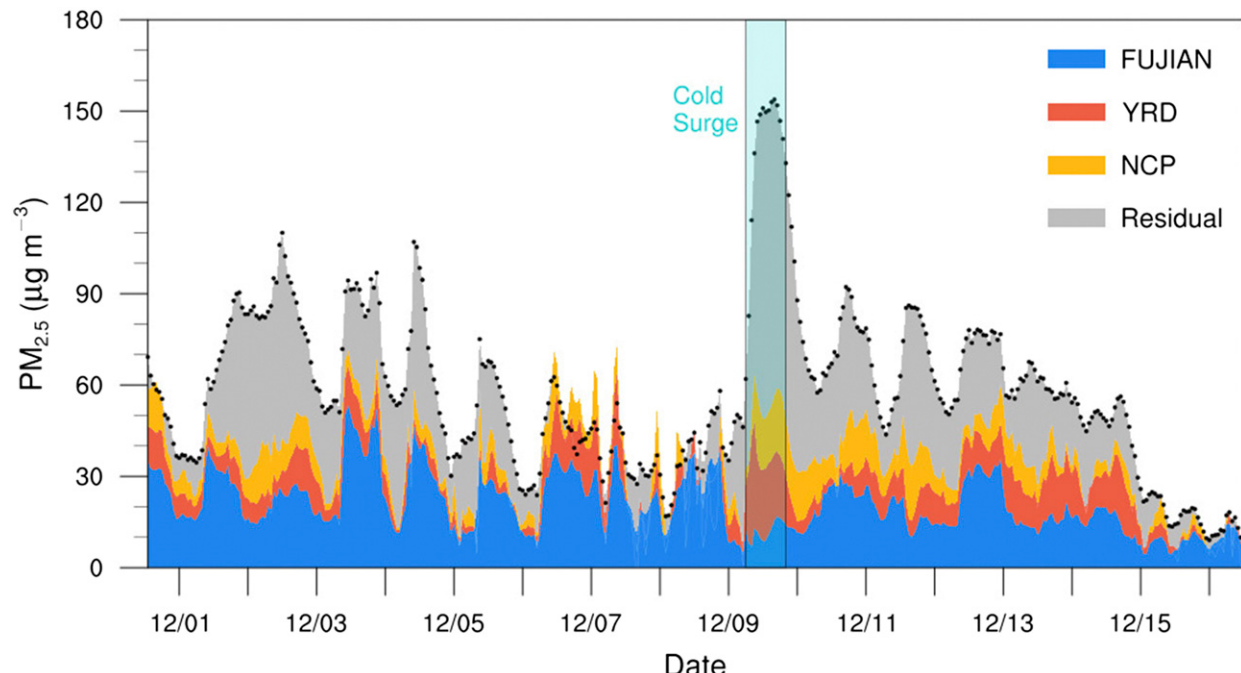


FIG. 12. Decomposition of the surface-layer  $\text{PM}_{2.5}$  concentrations ( $\mu\text{g m}^{-3}$ ) in Xiamen attributed to the linear additive components of contributions from anthropogenic emissions in FJ, YRD, and NCP (Fig. 1d), and the unidentified residual components associated with the chemical nonlinear responses to ARFs and the changes in precursor concentrations.

Although the above results demonstrate the importance of meteorological conditions and emission reduction scenarios on  $\text{PM}_{2.5}$  concentrations in Fujian Province, the results from this study are subject to uncertainties. Several known problems in model configuration, emission inventories, and boundary conditions will introduce inaccuracies and uncertainties in model performance and hence affect the magnitude of simulated aerosol concentrations and aerosol radiative feedbacks. Since AOD is underpredicted in eastern China, the simulated aerosol feedback may represent the lower limit. It has been suggested that the simulations in current atmospheric chemical models underpredict sulfate in northern China because of the lack of sulfate formation through transition-metal-catalyzed oxidation of  $\text{SO}_2$  in winter under low ambient temperature (Alexander et al. 2009; X. Huang et al. 2014; Zheng et al. 2015; Chen et al. 2016; Dong et al. 2016) and lack of the synergistic effect of  $\text{SO}_2$  and  $\text{NO}_2$  in high-humidity conditions (He et al. 2014; G. Wang et al. 2016). The MOSAIC aerosol module used in the current study does not simulate secondary organic aerosols, which is a limitation of the current study, but previous simulations including SOAs using the WRF-Chem model have been found to underestimate the winter organic carbon by a factor of 2 in mainland China, largely because of incomplete secondary organic aerosol

chemistry (Gao et al. 2014). All of these factors can underestimate aerosol radiative feedbacks in our simulations, which should be investigated in future studies.

*Acknowledgments.* This work was jointly supported by the External Cooperation Program of BIC, Chinese Academy of Sciences (Grant 134111KYSB20150016), the Public Benefiting Project of Xiamen Municipal Bureau of Science and Technology (Grant 3502z20164082), and the Scientific Research Foundation of the Third Institute of Oceanography, State Oceanic Administration of China (Grant 2011004).

## REFERENCES

- Abdul-Razzak, H., and S. J. Ghan, 2000: A parameterization of aerosol activation: 2. Multiple aerosol types. *J. Geophys. Res.*, **105**, 6837–6844, doi:[10.1029/1999JD901161](https://doi.org/10.1029/1999JD901161).
- , and —, 2002: A parameterization of aerosol activation 3. Sectional representation. *J. Geophys. Res.*, **107**, doi:[10.1029/2001JD000483](https://doi.org/10.1029/2001JD000483).
- Alexander, B., R. J. Park, D. J. Jacob, and S. Gong, 2009: Transition metal-catalyzed oxidation of atmospheric sulfur: Global implications for the sulfur budget. *J. Geophys. Res.*, **114**, D02309, doi:[10.1029/2008JD010486](https://doi.org/10.1029/2008JD010486).
- Chen, D., Z. Liu, J. Fast, and J. Ban, 2016: Simulations of sulfate-nitrate-ammonium (SNA) aerosols during the extreme haze events over northern China in October 2014. *Atmos. Chem. Phys.*, **16**, 10 707–10 724, doi:[10.5194/acp-16-10707-2016](https://doi.org/10.5194/acp-16-10707-2016).

- Chen, F., and J. Dudhia, 2001: Coupling an advanced land surface-hydrology model with the Penn State–NCAR MM5 modeling system. Part I: Model implementation and sensitivity. *Mon. Wea. Rev.*, **129**, 569–585, doi:10.1175/1520-0493(2001)129<0569:CAALSH>2.0.CO;2.
- Cheng, Z., J. Jiang, O. Fajardo, S. Wang, and J. Hao, 2013: Characteristics and health impacts of particulate matter pollution in China (2001–2011). *Atmos. Environ.*, **65**, 186–194, doi:10.1016/j.atmosenv.2012.10.022.
- Chuang, M.-T., J. S. Fu, C. J. Jang, C.-C. Chan, P.-C. Ni, and C.-T. Lee, 2008: Simulation of long-range transport aerosols from the Asian continent to Taiwan by a southward Asian high-pressure system. *Sci. Total Environ.*, **406**, 168–179, doi:10.1016/j.scitotenv.2008.07.003.
- Ding, A. J., and Coauthors, 2016: Enhanced haze pollution by black carbon in megacities in China. *Geophys. Res. Lett.*, **43**, 2873–2879, doi:10.1002/2016GL067745.
- Dong, X., J. S. Fu, K. Huang, D. Tong, and G. Zhuang, 2016: Model development of dust emission and heterogeneous chemistry within the Community Multiscale Air Quality modeling system and its application over East Asia. *Atmos. Chem. Phys.*, **16**, 8157–8180, doi:10.5194/acp-16-8157-2016.
- Draxler, R. R., and G. D. Hess, 1998: An overview of the HYSPLIT\_4 modelling system for trajectories, dispersion, and deposition. *Aust. Meteor. Mag.*, **47**, 295–308.
- Emmons, L. K., and Coauthors, 2010: Description and evaluation of the Model for Ozone and Related Chemical Tracers, version 4 (MOZART-4). *Geosci. Model Dev.*, **3**, 43–67, doi:10.5194/gmd-3-43-2010.
- Fast, J. D., W. I. Gustafson Jr., R. C. Easter, R. A. Zaveri, J. C. Barnard, E. G. Chapman, G. A. Grell, and S. E. Peckham, 2006: Evolution of ozone, particulates, and aerosol direct radiative forcing in the vicinity of Houston using a fully coupled meteorology–chemistry–aerosol model. *J. Geophys. Res.*, **111**, D21305, doi:10.1029/2005JD006721.
- , —, E. G. Chapman, R. C. Easter, J. P. Rishel, R. A. Zaveri, G. A. Grell, and M. C. Barth, 2011: The aerosol modeling testbed: A community tool to objectively evaluate aerosol process modules. *Bull. Amer. Meteor. Soc.*, **92**, 343–360, doi:10.1175/2010BAMS2868.1.
- , —, and Coauthors, 2012: Transport and mixing patterns over central California during the Carbonaceous Aerosol and Radiative Effects Study (CARES). *Atmos. Chem. Phys.*, **12**, 1759–1783, doi:10.5194/acp-12-1759-2012.
- , —, and Coauthors, 2014: Modeling regional aerosol and aerosol precursor variability over California and its sensitivity to emissions and long-range transport during the 2010 CalNex and CARES campaigns. *Atmos. Chem. Phys.*, **14**, 10 013–10 060, doi:10.5194/acp-14-10013-2014.
- Freitas, S. R., and Coauthors, 2007: Including the sub-grid scale plume rise of vegetation fires in low resolution atmospheric transport models. *Atmos. Chem. Phys.*, **7**, 3385–3398, doi:10.5194/acp-7-3385-2007.
- Gao, Y., C. Zhao, X. Liu, M. Zhang, and L. R. Leung, 2014: WRF-Chem simulations of aerosols and anthropogenic aerosol radiative forcing in East Asia. *Atmos. Environ.*, **92**, 250–266, doi:10.1016/j.atmosenv.2014.04.038.
- , M. Zhang, Z. Liu, L. Wang, P. Wang, X. Xia, M. Tao, and L. Zhu, 2015: Modeling the feedback between aerosol and meteorological variables in the atmospheric boundary layer during a severe fog–haze event over the North China Plain. *Atmos. Chem. Phys.*, **15**, 4279–4295, doi:10.5194/acp-15-4279-2015.
- Grell, G. A., S. E. Peckham, R. Schmitz, S. A. McKeen, G. Frost, W. C. Skamarock, and B. Eder, 2005: Fully coupled “online” chemistry within the WRF model. *Atmos. Environ.*, **39**, 6957–6975, doi:10.1016/j.atmosenv.2005.04.027.
- Guenther, A., T. Karl, P. Harley, C. Wiedinmyer, P. I. Palmer, and C. Geron, 2006: Estimates of global terrestrial isoprene emissions using MEGAN (Model of Emissions of Gases and Aerosols from Nature). *Atmos. Chem. Phys.*, **6**, 3181–3210, doi:10.5194/acp-6-3181-2006.
- Gustafson, W. I., Jr., E. G. Chapman, S. J. Ghan, R. C. Easter, and J. D. Fast, 2007: Impact on modeled cloud characteristics due to simplified treatment of uniform cloud condensation nuclei during NEAQS 2004. *Geophys. Res. Lett.*, **34**, L19809, doi:10.1029/2007GL030021.
- He, H., and Coauthors, 2014: Mineral dust and NOx promote the conversion of SO<sub>2</sub> to sulfate in heavy pollution days. *Sci. Rep.*, **4**, 4172, doi:10.1038/srep04172.
- Hsu, S. C., and Coauthors, 2010: High wintertime particulate matter pollution over an offshore island (Kinmen) off southeastern China: An overview. *J. Geophys. Res.*, **115**, D17309, doi:10.1029/2009JD013641.
- Huang, R.-J., and Coauthors, 2014: High secondary aerosol contribution to particulate pollution during haze events in China. *Nature*, **514**, 218–222, doi:10.1038/nature13774.
- Huang, X., Y. Song, C. Zhao, M. Li, T. Zhu, Q. Zhang, and X. Zhang, 2014: Pathways of sulfate enhancement by natural and anthropogenic mineral aerosols in China. *J. Geophys. Res. Atmos.*, **119**, 14 165–14 179, doi:10.1002/2014JD022301.
- Iacono, M. J., J. S. Delamere, E. J. Mlawer, M. W. Shephard, S. A. Clough, and W. D. Collins, 2008: Radiative forcing by long-lived greenhouse gases: Calculations with the AER radiative transfer models. *J. Geophys. Res.*, **113**, D13103, doi:10.1029/2008JD009944.
- Jiang, C., H. Wang, T. Zhao, T. Li, and H. Che, 2015: Modeling study of PM<sub>2.5</sub> pollutant transport across cities in China’s Jing–Jin–Ji region during a severe haze episode in December 2013. *Atmos. Chem. Phys.*, **15**, 5803–5814, doi:10.5194/acp-15-5803-2015.
- Jiang, F., Q. Liu, X. Huang, T. Wang, B. Zhuang, and M. Xie, 2012: Regional modeling of secondary organic aerosol over China using WRF/Chem. *J. Aerosol Sci.*, **43**, 57–73, doi:10.1016/j.jaerosci.2011.09.003.
- Kaufman, Y. J., and Coauthors, 2005: A critical examination of the residual cloud contamination and diurnal sampling effects on MODIS estimates of aerosol over ocean. *IEEE Trans. Geosci. Remote Sens.*, **43**, 2886–2897, doi:10.1109/TGRS.2005.858430.
- Li, M., and Coauthors, 2017: MIX: A mosaic Asian anthropogenic emission inventory under the international collaboration framework of the MICS-Asia and HTAP. *Atmos. Chem. Phys.*, **17**, 935–963, doi:10.5194/acp-17-935-2017.
- Lin, Y.-L., R. D. Farley, and H. D. Orville, 1983: Bulk parameterization of the snow field in a cloud model. *J. Climate Appl. Meteor.*, **22**, 1065–1092, doi:10.1175/1520-0450(1983)022<1065:BPOTSF>2.0.CO;2.
- Massey, J. D., W. J. Steenburgh, J. C. Knievel, and W. Y. Y. Cheng, 2016: Regional soil moisture biases and their influence on WRF model temperature forecasts over the Intermountain West. *Wea. Forecasting*, **31**, 197–216, doi:10.1175/WAF-D-15-0073.1.
- Mlawer, E. J., S. J. Taubman, P. D. Brown, M. J. Iacono, and S. A. Clough, 1997: Radiative transfer for inhomogeneous atmospheres: RRTM, a validated correlated-k model for the

- longwave. *J. Geophys. Res.*, **102**, 16 663–16 682, doi:[10.1029/97JD00237](https://doi.org/10.1029/97JD00237).
- Ngan, F., H. Kim, P. Lee, K. Al-Wali, and B. Dornblaser, 2013: A study of nocturnal surface wind speed overprediction by the WRF-ARW model in southeastern Texas. *J. Appl. Meteor. Climatol.*, **52**, 2638–2653, doi:[10.1175/JAMC-D-13-060.1](https://doi.org/10.1175/JAMC-D-13-060.1).
- Niu, F., Z. Li, C. Li, K.-H. Lee, and M. Wang, 2010: Increase of wintertime fog in China: Potential impacts of weakening of the eastern Asian monsoon circulation and increasing aerosol loading. *J. Geophys. Res.*, **115**, D00K20, doi:[10.1029/2009JD013484](https://doi.org/10.1029/2009JD013484).
- Niu, Z., F. Zhang, J. Chen, L. Yin, S. Wang, and L. Xu, 2013: Carbonaceous species in PM<sub>2.5</sub> in the coastal urban agglomeration in the western Taiwan Strait region, China. *Atmos. Res.*, **122**, 102–110, doi:[10.1016/j.atmosres.2012.11.002](https://doi.org/10.1016/j.atmosres.2012.11.002).
- Pleim, J. E., 2007: A combined local and nonlocal closure model for the atmospheric boundary layer. Part I: Model description and testing. *J. Appl. Meteor. Climatol.*, **46**, 1383–1395, doi:[10.1175/JAM2539.1](https://doi.org/10.1175/JAM2539.1).
- Qu, W. J., R. Arimoto, X. Y. Zhang, C. H. Zhao, Y. Q. Wang, L. F. Sheng, and G. Fu, 2010: Spatial distribution and interannual variation of surface PM<sub>10</sub> concentrations over eighty-six Chinese cities. *Atmos. Chem. Phys.*, **10**, 5641–5662, doi:[10.5194/acp-10-5641-2010](https://doi.org/10.5194/acp-10-5641-2010).
- , J. Wang, X. Zhang, Z. Yang, and S. Gao, 2015: Effect of cold wave on winter visibility over eastern China. *J. Geophys. Res. Atmos.*, **120**, 2394–2406, doi:[10.1002/2014JD021958](https://doi.org/10.1002/2014JD021958).
- Remer, L. A., and Coauthors, 2005: The MODIS aerosol algorithm, products, and validation. *J. Atmos. Sci.*, **62**, 947–973, doi:[10.1175/JAS3385.1](https://doi.org/10.1175/JAS3385.1).
- Sun, Y., O. Jiang, Z. Wang, P. Fu, J. Li, T. Yang, and Y. Yin, 2014: Investigation of the sources and evolution processes of severe haze pollution in Beijing in January 2013. *J. Geophys. Res. Atmos.*, **119**, 4380–4398, doi:[10.1002/2014JD021641](https://doi.org/10.1002/2014JD021641).
- Tang, L., and Coauthors, 2016: Regional contribution to PM<sub>1</sub> pollution during winter haze in Yangtze River delta, China. *Sci. Total Environ.*, **541**, 161–166, doi:[10.1016/j.scitotenv.2015.05.058](https://doi.org/10.1016/j.scitotenv.2015.05.058).
- Vautard, R., and Coauthors, 2012: Evaluation of the meteorological forcing used for the Air Quality Model Evaluation International Initiative (AQMEII) air quality simulations. *Atmos. Environ.*, **53**, 15–37, doi:[10.1016/j.atmosenv.2011.10.065](https://doi.org/10.1016/j.atmosenv.2011.10.065).
- Wang, G., and Coauthors, 2016: Persistent sulfate formation from London fog to Chinese haze. *Proc. Natl. Acad. Sci. USA*, **113**, 13 630–13 635, doi:[10.1073/pnas.1616540113](https://doi.org/10.1073/pnas.1616540113).
- Wang, S.-H., W.-T. Hung, S.-C. Chang, and M.-C. Yen, 2016: Transport characteristics of Chinese haze over northern Taiwan in winter, 2005–2014. *Atmos. Environ.*, **126**, 76–86, doi:[10.1016/j.atmosenv.2015.11.043](https://doi.org/10.1016/j.atmosenv.2015.11.043).
- Wiedinmyer, C., S. K. Akagi, R. J. Yokelson, L. K. Emmons, J. A. Al-Saadi, J. J. Orlando, and A. J. Soja, 2011: The Fire Inventory from NCAR (FINN): A high resolution global model to estimate the emissions from open burning. *Geosci. Model Dev.*, **4**, 625–641, doi:[10.5194/gmd-4-625-2011](https://doi.org/10.5194/gmd-4-625-2011).
- Xu, L., and Coauthors, 2013: Spatial distribution and sources identification of elements in PM<sub>2.5</sub> among the coastal city group in the western Taiwan Strait region, China. *Sci. Total Environ.*, **442**, 77–85, doi:[10.1016/j.scitotenv.2012.10.045](https://doi.org/10.1016/j.scitotenv.2012.10.045).
- Yan, J., L. Chen, Q. Lin, Z. Li, H. Chen, and S. Zhao, 2015: Chemical characteristics of submicron aerosol particles during a long-lasting haze episode in Xiamen, China. *Atmos. Environ.*, **113**, 118–126, doi:[10.1016/j.atmosenv.2015.05.003](https://doi.org/10.1016/j.atmosenv.2015.05.003).
- Yang, F., and Coauthors, 2011: Characteristics of PM<sub>2.5</sub> speciation in representative megacities and across China. *Atmos. Chem. Phys.*, **11**, 5207–5219, doi:[10.5194/acp-11-5207-2011](https://doi.org/10.5194/acp-11-5207-2011).
- Yin, L., Z. Niu, X. Chen, J. Chen, F. Zhang, and L. Xu, 2014: Characteristics of water-soluble inorganic ions in PM<sub>2.5</sub> and PM<sub>2.5–10</sub> in the coastal urban agglomeration along the western Taiwan Strait region, China. *Environ. Sci. Pollut. Res.*, **21**, 5141–5156, doi:[10.1007/s11356-013-2134-7](https://doi.org/10.1007/s11356-013-2134-7).
- Yu, S., Q. Zhang, R. Yan, S. Wang, P. Li, B. Chen, W. Liu, and X. Zhang, 2014: Origin of air pollution during a weekly heavy haze episode in Hangzhou, China. *Environ. Chem. Lett.*, **12**, 543–550, doi:[10.1007/s10311-014-0483-1](https://doi.org/10.1007/s10311-014-0483-1).
- Zaveri, R. A., and L. K. Peters, 1999: A new lumped structure photochemical mechanism for large-scale applications. *J. Geophys. Res.*, **104**, 30 387–30 415, doi:[10.1029/1999JD900876](https://doi.org/10.1029/1999JD900876).
- , R. C. Easter, J. D. Fast, and L. K. Peters, 2008: Model for Simulating Aerosol Interactions and Chemistry (MOSAIC). *J. Geophys. Res.*, **113**, D13204, doi:[10.1029/2007JD008782](https://doi.org/10.1029/2007JD008782).
- Zhang, B., Y. Wang, and J. Hao, 2015: Simulating aerosol–radiation–cloud feedbacks on meteorology and air quality over eastern China under severe haze conditions in winter. *Atmos. Chem. Phys.*, **15**, 2387–2404, doi:[10.5194/acp-15-2387-2015](https://doi.org/10.5194/acp-15-2387-2015).
- Zhang, F., L. Xu, J. Chen, Y. Yu, Z. Niu, and L. Yin, 2012: Chemical compositions and extinction coefficients of PM<sub>2.5</sub> in peri-urban of Xiamen, China, during June 2009–May 2010. *Atmos. Res.*, **106**, 150–158, doi:[10.1016/j.atmosres.2011.12.005](https://doi.org/10.1016/j.atmosres.2011.12.005).
- Zhang, H., Z. Pu, and X. Zhang, 2013: Examination of errors in near-surface temperature and wind from WRF numerical simulations in regions of complex terrain. *Wea. Forecasting*, **28**, 893–914, doi:[10.1175/WAF-D-12-00109.1](https://doi.org/10.1175/WAF-D-12-00109.1).
- Zhang, X. Y., Y. Q. Wang, T. Niu, X. C. Zhang, S. L. Gong, Y. M. Zhang, and J. Y. Sun, 2012: Atmospheric aerosol compositions in China: Spatial/temporal variability, chemical signature, regional haze distribution and comparisons with global aerosols. *Atmos. Chem. Phys.*, **12**, 779–799, doi:[10.5194/acp-12-779-2012](https://doi.org/10.5194/acp-12-779-2012).
- Zhang, Y., A. Ding, H. Mao, W. Nie, D. Zhou, L. Liu, X. Huang, and C. Fu, 2016a: Impact of synoptic weather patterns and inter-decadal climate variability on air quality in the North China Plain during 1980–2013. *Atmos. Environ.*, **124**, 119–128, doi:[10.1016/j.atmosenv.2015.05.063](https://doi.org/10.1016/j.atmosenv.2015.05.063).
- , X. Zhang, L. Wang, Q. Zhang, F. Duan, and K. He, 2016b: Application of WRF/Chem over East Asia: Part I. Model evaluation and intercomparison with MM5/CMAQ. *Atmos. Environ.*, **124**, 285–300, doi:[10.1016/j.atmosenv.2015.07.022](https://doi.org/10.1016/j.atmosenv.2015.07.022).
- Zhao, J., F. Zhang, Y. Xu, and J. Chen, 2011: Characterization of water-soluble inorganic ions in size-segregated aerosols in coastal city, Xiamen. *Atmos. Res.*, **99**, 546–562, doi:[10.1016/j.atmosres.2010.12.017](https://doi.org/10.1016/j.atmosres.2010.12.017).
- Zhao, X. J., P. S. Zhao, J. Xu, W. Meng, W. W. Pu, F. Dong, D. He, and Q. F. Shi, 2013: Analysis of a winter regional haze event and its formation mechanism in the North China Plain. *Atmos. Chem. Phys.*, **13**, 5685–5696, doi:[10.5194/acp-13-5685-2013](https://doi.org/10.5194/acp-13-5685-2013).
- Zheng, B., and Coauthors, 2015: Heterogeneous chemistry: A mechanism missing in current models to explain secondary inorganic aerosol formation during the January 2013 haze episode in North China. *Atmos. Chem. Phys.*, **15**, 2031–2049, doi:[10.5194/acp-15-2031-2015](https://doi.org/10.5194/acp-15-2031-2015).